

An Observational Study of Environmental Influences on the Intensity Changes of Typhoons Flo (1990) and Gene (1990)

CHUN-CHIEH WU AND HSIU-JU CHENG

Department of Atmospheric Sciences, National Taiwan University, Taipei, Taiwan

(Manuscript received 27 July 1998, in final form 22 December 1998)

ABSTRACT

The European Centre for Medium-Range Weather Forecasts Tropical Ocean–Global Atmosphere advanced analysis was used to study the mechanisms that affect the intensity of Typhoons Flo (1990) and Gene (1990). The outflow structure, eddy momentum flux convergence, and the mean vertical wind shear were examined.

The evolution of potential vorticity (PV) in the outflow layer showed low PV areas on top of both Typhoons Flo and Gene, and the low PV areas expanded as the typhoons intensified. The outflow pattern of the two typhoons was influenced by the upper-tropospheric environmental systems. The upper-level environmental features were shown to play a crucial role in the intensification of the two typhoons.

The tropical upper-tropospheric trough cell east of Flo provided the outflow channel for the typhoon. The enhanced outflow, the upper-level eddy flux convergence (EFC), the low vertical wind shear, and the warm sea surface temperature provided all favorable conditions for the development of Flo. On the other hand, the intensification of Gene was associated with its interaction with an upper-level midlatitude trough. The approach of the trough produced upper-level EFC of angular momentum outside 10° lat radius, and the EFC shifted inward with time. As the EFC shifted into the vicinity of the storm core, Gene started to intensify steadily until the midlatitude trough passed over.

The intensifying processes of the above cases indicate the importance of the upper-tropospheric systems to the intensity change of typhoons. The influence of upper-level environmental systems on the tropical cyclones is prominent in the low inertial stability outflow layer. However, results from the piecewise PV inversion of the upper-level environmental PV anomalies showed little evidence that the intensification of both typhoons were directly associated with the superposition of PV anomalies.

1. Introduction

Tropical cyclones are destructive weather systems. Onslaught by a severe tropical cyclone on human residences usually results in serious property damage and sometimes heavy loss of life. Although numerical models have shown considerable skill (e.g., Kurihara et al. 1998) in tropical cyclone track forecasting, the prediction of tropical cyclone intensity remains a highly challenging task for meteorologists and weather forecasters. For example, Avila (1998) has shown that no significant improvement in the official intensity forecast was made at the National Hurricane Center for the Atlantic basin between 1990 and 1997. It is clear that to improve the prediction of tropical cyclone intensity, extensive research is required for a greater understanding of the structure and evolution of a tropical cyclone and to identify the key mechanisms controlling the change in intensity of tropical cyclones.

The intensity of a typhoon, as conventionally measured by its maximum surface wind or minimum surface pressure, is affected at any time by large and complex arrays of physical processes that govern the interaction of the storm both with the underlying ocean and with its atmospheric environment. In general, the factors affecting the intensity of tropical cyclones can be categorized into three areas: 1) upper-ocean (air–sea) interaction, 2) internal eyewall (storm core) dynamics, and 3) atmospheric–environmental interaction. The backgrounds of past studies on these factors affecting typhoon intensity are reviewed here.

a. Upper-ocean (air–sea) interaction

It is well known that the ocean is a large energy reservoir for tropical cyclones. Thus sea surface temperature (SST) plays a crucial role in the determination of the maximum intensity of a tropical cyclone. On this basis, Merrill (1988) derived an empirical maximum intensity of tropical cyclone for a given SST. Moreover, a theoretical upper bound of intensity that a tropical cyclone can achieve has been determined using SST and the atmospheric thermodynamic environment (Emanuel

Corresponding author address: Dr. Chun-Chieh Wu, Dept. of Atmospheric Sciences, National Taiwan University, 61, Ln. 144, Sec. 4, Keelung Rd., Taipei 10772, Taiwan.
E-mail: cwu@typhoon.as.ntu.edu.tw

1986), whereby a tropical cyclone is regarded as a Carnot heat engine, gaining energy from the disequilibrium between the air and ocean surface. This air–sea interaction theory for tropical cyclones has been further elaborated in Emanuel (1988, 1991, 1995). Another thermodynamic approach to estimating the maximum potential intensity (MPI) of tropical cyclones has also been described by Holland (1997). The feedback of ocean on the intensity of tropical cyclones has been examined in the hurricane–ocean coupled model (e.g., Bender et al. 1993). A case in point is the rapid intensification of Hurricane Opal (1995) near and across a warm-core eddy over the warm sector of the Gulf of Mexico (Shay et al. 1998; Black and Shay 1998; Bosart et al. 1998).

b. Internal eyewall dynamics

Besides the SST factor, the eyewall dynamics also control the intensity evolution in tropical cyclones (e.g., Willoughby et al. 1982; Shapiro and Willoughby 1982; Willoughby and Black 1996). However, many aspects of eyewall behavior have not been fully understood. The response of the tropical cyclone intensity to the convective and microphysical processes in the eyewall region is not well explained. A recent theoretical study (Montgomery and Kallenbach 1997; Montgomery 1998) employing the potential vorticity (PV) concept is illuminating. However, until detailed and precise measurements within the eyewall can be obtained, the complicated eyewall dynamics and its relation with tropical cyclone intensity may remain a mystery.

c. Atmospheric–environmental interaction

1) THE ROLE OF EDDY FLUX CONVERGENCE (EFC)

While the interaction between the internal (core) dynamics and tropical cyclone intensity is more difficult to understand, both observational and numerical studies have paid much attention to the external atmospheric influences (especially the upper-tropospheric interaction) on tropical cyclone intensity. Pfeffer and Challa (1981) used the observations from the Atlantic developing and nondeveloping tropical disturbances composited by McBride (1981a,b) and McBride and Zehr (1981) to examine the importance of large-scale eddy fluxes of momentum in the development of the storms in their model. Pfeffer and Challa (1981) concluded that a sufficiently intense and properly organized EFC of momentum is an essential ingredient for the development of Atlantic tropical disturbances into hurricanes.

The relationship between EFC of angular momentum and tropical cyclone intensity for the named tropical cyclones during the 1989–91 Atlantic hurricane seasons was investigated by DeMaria et al. (1993). They showed that about one-third of the storms with enhanced EFC of angular momentum intensified just after the period of enhanced EFC. Most of the storms that did not in-

tensify after the enhanced EFC usually experienced increasing vertical shears, moved over cool water, or became extratropical. Their results indicated that in addition to SST, EFC and vertical wind shear are also crucial factors that affect the intensity of a tropical cyclone.

The work of Pfeffer and Challa (1981) focused on the importance of eddy momentum forcing to the initial development of a tropical cyclone. Molinari and Vollaro (1989, 1990) found that upper-level EFC of angular momentum occurred during the intensifying period of Hurricane Elena (1985), indicating that the upper-tropospheric trough played an important role in the reintensification of Elena. The European Centre for Medium-Range Weather Forecasts (ECMWF) analyses on a 2.5° lat \times 2.5° long grid were used by Molinari and Vollaro (1990) to evaluate the response of the Eliassen's balanced vortex to momentum and heat fluxes. The balanced vortex solution showed an in–up–out circulation that shifted inward with time, which is consistent with the inward propagation of the maximum outflow found by Molinari and Vollaro (1989). This result also indicated the environmental control on the behavior of the storm.

2) OUTFLOW STRUCTURE

The inertial stability in a tropical cyclone is lower in the outflow layer than that in the middle and lower layers (Holland and Merrill 1984). Because of the low inertial stability in the outflow layer, the influence of upper-level environmental forcing may extend to the inner parts of a tropical cyclone more easily. Holland and Merrill (1984) showed that the radial–vertical circulation induced by the upper-level momentum forcing has a direct and substantial effect on the core region of a tropical cyclone. They also proposed that the cooperative interaction between a tropical cyclone and a passing trough can enhance the outflow jet of a tropical cyclone. The enhanced outflow jet can invigorate core region convection and initiate the deepening process of the cyclone.

The asymmetric structures of the outflow layer reflect the influences from the upper-level environmental systems, and these structures can produce the large eddy imports of angular momentum. The vertical derivative of the EFC of angular momentum acts as a forcing function to increase inflow of moist air into the boundary layer and to pump drier air out into the outflow layer (Challa and Pfeffer 1980). Challa and Pfeffer (1980) used Sundqvist's (1970) axisymmetric model to simulate the responses of a vortex to different profiles of momentum forcing and found that numerical simulations with the environmental forcing could produce more rapid intensification and more intense tropical storms.

Merrill and Velden (1996) used rawinsondes and cloud motion wind vectors derived from geostationary

satellite imagery to describe the three-dimensional structure of the outflow layer of Supertyphoon Flo (1990). The net outflow at 6° lat was found to occur at higher levels and over an increasing range of potential temperature surfaces as Flo intensified. The result is consistent with the conceptual model proposed by Emanuel (1986). In the Emanuel model, the air flows inward in the boundary layer at constant temperature, then ascends along the constant potential temperature surfaces (as well as constant angular momentum surfaces), and finally gives off heat at a much lower temperature in the lower stratosphere or upper troposphere. Due to the temperature gradient inside the storm, air ascending in the eyewall should emanate at a higher potential temperature than air ascending in the peripheral convection of the storm. Merrill and Velden (1996) suggested that the enhanced EFC during the period after Flo's peak intensity may have stimulated the outflow at the θ level below the eyewall outflow, which favored more convection outside the eyewall and impeded the development of Flo.

3) VERTICAL WIND SHEAR

Besides the EFC of angular momentum, the interaction between the tropical cyclone and the upper-tropospheric trough also increased the vertical wind shear. Molinari et al. (1995) proposed that the interaction between the outflow from Elena (1985) and an upper-tropospheric trough reduced the penetration depth of the upper-level westerlies and the length of time during which the vertical wind shear occurred, thus preventing the destruction of Elena by the shear. Molinari et al. (1995) further suggested that the partial superposition of the upper-tropospheric trough on Elena initiated the wind-induced surface heat exchange (WISHE) mechanism (Emanuel 1991), which resulted in the reintensification of the storm. Similar argument was also presented for the case study of Hurricane Danny (1985) in Molinari et al. (1998).

It has been shown in earlier observational studies (e.g., Gray 1968; Merrill 1988) that the vertical shear of a horizontal wind has a negative influence on the intensification of tropical cyclones. A common explanation of the effect of vertical wind shear is that the heat of condensation released at upper levels is advected in a different direction relative to the heat released at lower levels and therefore the "ventilation" of heat away from the circulation inhibits the development of the storm (Gray 1968). In addition to the idea of ventilation, a clever explanation concerning the effect of vertical wind shear on tropical cyclone intensity was proposed by DeMaria (1996). A simple two-layer model was used to show that the tilt of the upper- and lower-level PV produces a midlevel temperature decrease in the direction of the displaced upper PV and a temperature increase near the vortex center. This kind of midlevel temperature perturbation can act to increase con-

vection away from the storm center and thus inhibits storm development. The resistance of a vortex to vertical wind shear is a function of the Rossby penetration depth, which increases with the latitude, horizontal scale, and vortex amplitude. In the regression analyses, DeMaria (1996) demonstrated that high-latitude, large, and intense tropical cyclones tend to be less sensitive to the effect of vertical shear than low-latitude, small, and weak storms.

d. Objectives

The aforementioned studies have pointed out the importance of EFC, vertical wind shear, SST, and eyewall dynamics to the intensity change of tropical cyclones. In this paper, the above three factors are evaluated to study the environmental influences on the intensity change of Typhoons Flo (1990) and Gene (1990), using the ECMWF Tropical Ocean–Global Atmosphere (TOGA) advanced global analysis and the National Centers for Environmental Prediction (NCEP) SST analysis. Unfortunately, due to data limitations, the effect of eyewall convection is not investigated here.

The use of operational analyses for investigating tropical cyclone intensity and the interaction between a tropical cyclone and its environment has been well documented in Molinari and Vollaro (1990), Molinari et al. (1992), and Molinari et al. (1995). Molinari et al. (1992) used both the ECMWF high-resolution ($1.125^\circ \times 1.125^\circ$) uninitialized and the lower-resolution ($2.5^\circ \times 2.5^\circ$) initialized analyses to study the outflow structure of Hurricane Allen (1980) and Hurricane Elena (1985). They found that the azimuthal mean tangential velocity around the storms was well represented in both analyses, but that the azimuthal mean radial velocity was poorly represented. Despite the poor analysis in radial velocity, the azimuthal eddy flux of angular momentum was well reproduced in both ECMWF analyses. It is emphasized that the advantage of using operational analyses for case studies of tropical cyclones is that it provides more information over the ocean and regions with sparse rawinsonde data.

Meanwhile, previous studies have applied the PV perspective to study tropical cyclone motion and the characteristics of tropical cyclone outflow. Wu and Emanuel (1993) showed that the upper-level low PV air is displaced downshear from the lower point vortex as a result of the ambient vertical shear, and thus the mutual interaction between the circulations associated with the upper- and lower-level PV anomalies may cause the lower-level vortex to drift to the left of the vertical shear vector. Wu and Emanuel (1994) also found that the interaction of the baroclinic vortex with background vertical shear may produce a jetlike outflow structure. Merrill and Velden (1996) showed that the largest negative PV tendency was apparent near the level of maximum outflow in Typhoon Flo. In our study, the evolution of PV in the outflow region was investigated to understand

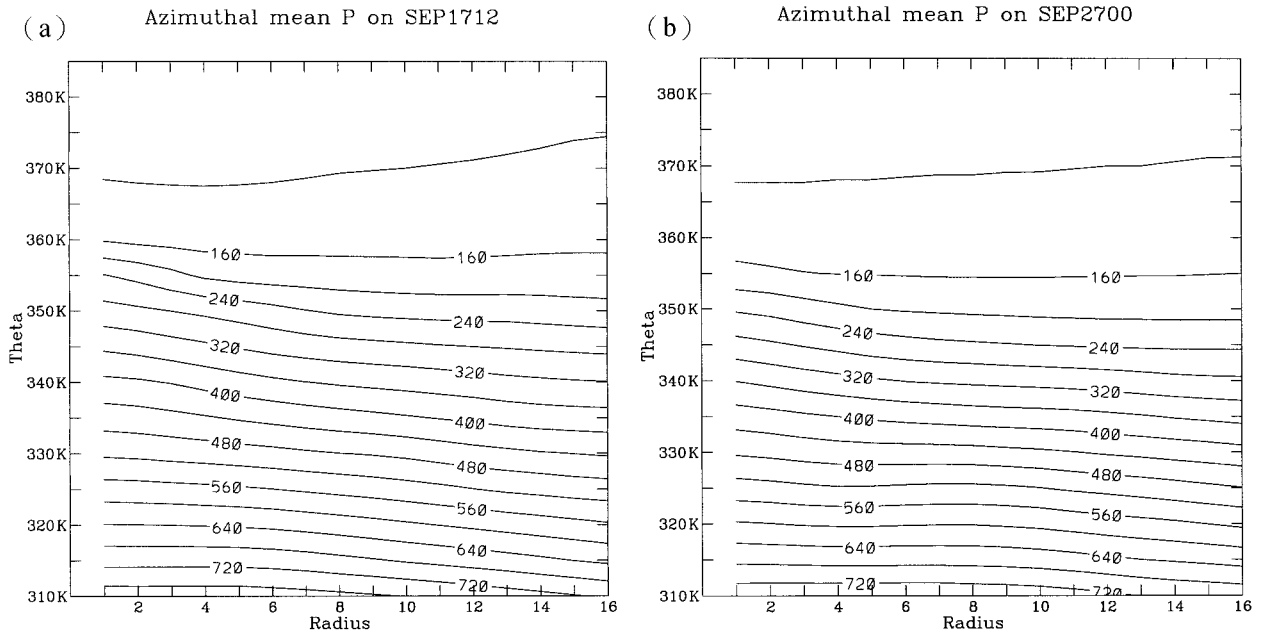


FIG. 1. Axisymmetric means of ECMWF TOGA advanced analyses of pressure on isentropic surfaces in cylindrical coordinates centered on the center of (a) Typhoon Flo (1990) at 1200 UTC 17 Sep, (b) Typhoon Gene (1990) at 0000 UTC 27 Sep.

the outflow structure and the interaction between the upper-level environmental features and the storms. To take account of the effects of eddy heat fluxes during the interaction periods, the Eliassen–Palm fluxes were also calculated.

The data and analysis methods are introduced in section 2. Results for case studies of Typhoons Flo and Gene are presented in sections 3 and 4, respectively. The effects from all factors affecting the intensity change of each typhoon are also discussed and compared with each other in section 5. The concluding remarks of this study are drawn in section 6.

2. Data and methodology

a. Data

The ECMWF TOGA global analysis is the operational analysis from the ECMWF. The 6-hourly ECMWF TOGA advanced upper-level analyses on $1.125^\circ \text{ lat} \times 1.125^\circ \text{ long}$ grids are available at 14 pressure levels: 1000, 850, 700, 500, 400, 300, 250, 200, 150, 100, 70, 50, 30, and 10 hPa. Twelve of the fourteen levels (between 1000 and 50 hPa) from the ECMWF TOGA advanced upper-level analyses were employed in this work. The sea surface temperature along the typhoon track was determined by the NCEP SST analysis, which is produced weekly with a 1° resolution.

b. Methodology

The analyses in this study contain calculations of PV, EFC of relative angular momentum, Eliassen–Palm

flux, and mean vertical shear. In addition, the azimuthal mean of the typhoon-relative radial and tangential wind, and the PV on both isobaric and isentropic levels are also obtained. Isobars on potential temperature versus radius plots for the two case studies are shown in Fig. 1.

1) POTENTIAL VORTICITY ANALYSIS

The PV evolution in the outflow layer is adopted to study the outflow structure and the interaction between each typhoon and its associated upper-level environmental features. Ertel's PV is defined as

$$\text{PV} = \frac{\boldsymbol{\zeta}_a \cdot \nabla \theta}{\rho},$$

where $\boldsymbol{\zeta}_a$ is the absolute vorticity vector, θ is the potential temperature, and ρ is the density.

In isentropic coordinates, PV is given by

$$\text{PV} = -g \left(\frac{\partial p}{\partial \theta} \right)^{-1} \left[f + \left(\frac{\partial v}{\partial x} \right)_\theta - \left(\frac{\partial u}{\partial y} \right)_\theta \right], \quad (1)$$

where p is the pressure, θ is the potential temperature, f is the Coriolis parameter, u is the zonal wind, v is the meridional wind, and the subscript θ denotes the derivative taken along θ surfaces. In the calculation of PV we choose the lowest θ surface at 310 K, which is about the lowest level not intercepting the ground. We also choose 385 K as the top potential temperature level.

2) EDDY FLUX CONVERGENCE OF ANGULAR MOMENTUM

Following Molinari and Vollaro (1990), the EFC of relative angular momentum is defined as

$$\text{EFC} = -\frac{1}{r^2} \frac{\partial}{\partial r} r^2 \overline{u'_L v'_L}, \quad (2)$$

where u_L is the storm-relative radial velocity, v_L is the storm-relative tangential velocity, r is the radius, the overbar denotes the azimuthal mean, and the prime indicates the deviation from the azimuthal mean.

3) ELIASSEN–PALM FLUX

In addition to the eddy flux of momentum, the eddy heat flux may also play a role in the development of tropical cyclones. Both the eddy flux of momentum and heat can be combined in one form—the Eliassen–Palm (E–P) flux. Following Molinari et al. (1995), the E–P flux divergence can be written as

$$\nabla \cdot \mathbf{F} = -\frac{1}{r} \frac{\partial}{\partial r} r^2 \overline{(\sigma u_L)' v'_L} + \frac{\partial}{\partial \theta} p' \frac{\partial \Psi'}{\partial \lambda}, \quad (3)$$

where

$$\mathbf{F} \equiv \left[-r \overline{(\sigma u_L)' v'_L}, p' \frac{\partial \Psi'}{\partial \lambda} \right] \quad (4)$$

is the E–P flux vector, $\sigma = -\partial p / \partial \theta$ is the pseudodensity, u_L is the storm-relative radial velocity, v_L is the storm-relative tangential velocity, θ is the potential temperature, Ψ is the Montgomery streamfunction, and λ is the azimuthal angle. The radial component of E–P flux represents the angular momentum flux, while the vertical component is the heat flux. Here, the E–P flux is calculated on cylindrical coordinates, and the overbar represents the azimuthal mean.

The calculation of EFC and E–P flux is made using storm-relative cylindrical coordinates with $\Delta r = 0.5$ lat and $\Delta \lambda = 15^\circ$. The EFC was calculated on each mandatory isobaric surface and the E–P flux divergence was evaluated on isentropic coordinates with a 5 K vertical resolution.

4) VERTICAL WIND SHEAR

Two different methods were used for evaluating the mean vertical wind shear. First, the vertical wind shear was obtained by taking the vector difference of the annular mean wind within a $5^\circ \sim 7^\circ$ radius between 200 hPa and 850 hPa (hereafter referred to as A method). In addition, a three-point smoothing operator (Kurihara et al. 1993) was applied to determine the environmental wind field. The vector difference of the environmental wind at the typhoon center between 200 hPa and 850 hPa represents the second type (hereafter referred to as

K method) of the environmental vertical wind shear in our study.

3. Supertyphoon Flo

Flo formed southeast of Guam, and reached typhoon strength at 0600 UTC 15 September 1990. Thereafter Flo intensified rapidly and became a supertyphoon at 1200 UTC 16 September. The intensity and track recorded by the Joint Typhoon Warning Center (JTWC), and the NCEP weekly mean SST during the evolution of Flo are shown in Fig. 2. Flo moved northwestward steadily before recurving around the western edge of the subtropical ridge. As shown in Fig. 2, the peak intensity of Flo was observed at 0600 UTC 17 September with a maximum surface wind of 145 kt, and a central pressure of 891 hPa. After reaching peak intensity, Flo accelerated northeastward and made landfall in Japan on 19 September. Maximum intensity was maintained for 6 h and then Flo decayed rapidly.

The analyses in this section are based on the ECMWF TOGA advanced $1.125^\circ \times 1.125^\circ$ gridded analyses. The axisymmetric structure of Typhoon Flo is first introduced, followed by the analyses of PV and wind fields on isentropic surfaces in the outflow layer. Then the E–P flux divergence, the EFC of angular momentum, and the vertical wind shear are calculated to investigate the interaction between the upper-level environmental systems and Flo. The evolution of Flo is also analyzed in three different periods of interest: 1) the rapid-intensification stage, from 0000 UTC 15 September to 1200 UTC 16 September; 2) the mature stage, which is defined as the period after Flo became a supertyphoon and intensified to the maximum intensity, from 1200 UTC 16 September to 1200 UTC 17 September; and 3) the decaying stage, from 1200 UTC 17 September to 1800 UTC 18 September, when Flo weakened rapidly after reaching peak intensity.

a. Axisymmetric structure

First, the azimuthal mean was taken to represent the axisymmetric structure of Flo. The axisymmetric cross section of the radial and tangential winds during Flo's peak intensity (1200 UTC 17 September) are shown in Fig. 3. The axisymmetric wind structure of Flo demonstrates a low-level inflow and an upper-tropospheric outflow. The cyclonic tangential wind near the storm center extended up to 370 K. The maximum radial outflow is located at 8° radius on 360 K, while the radius of the maximum tangential wind in the gridded analyses is at about 3° . This large radius of maximum wind reflects the limitation of the large-scale analyses in capturing the inner structure of Flo.

The radius and potential temperature (r – θ) cross section of 24-h average axisymmetric PV (bold solid contours) and the 24-h axisymmetric PV tendency (the rate of change in azimuthal mean PV for a 24-h period; thin

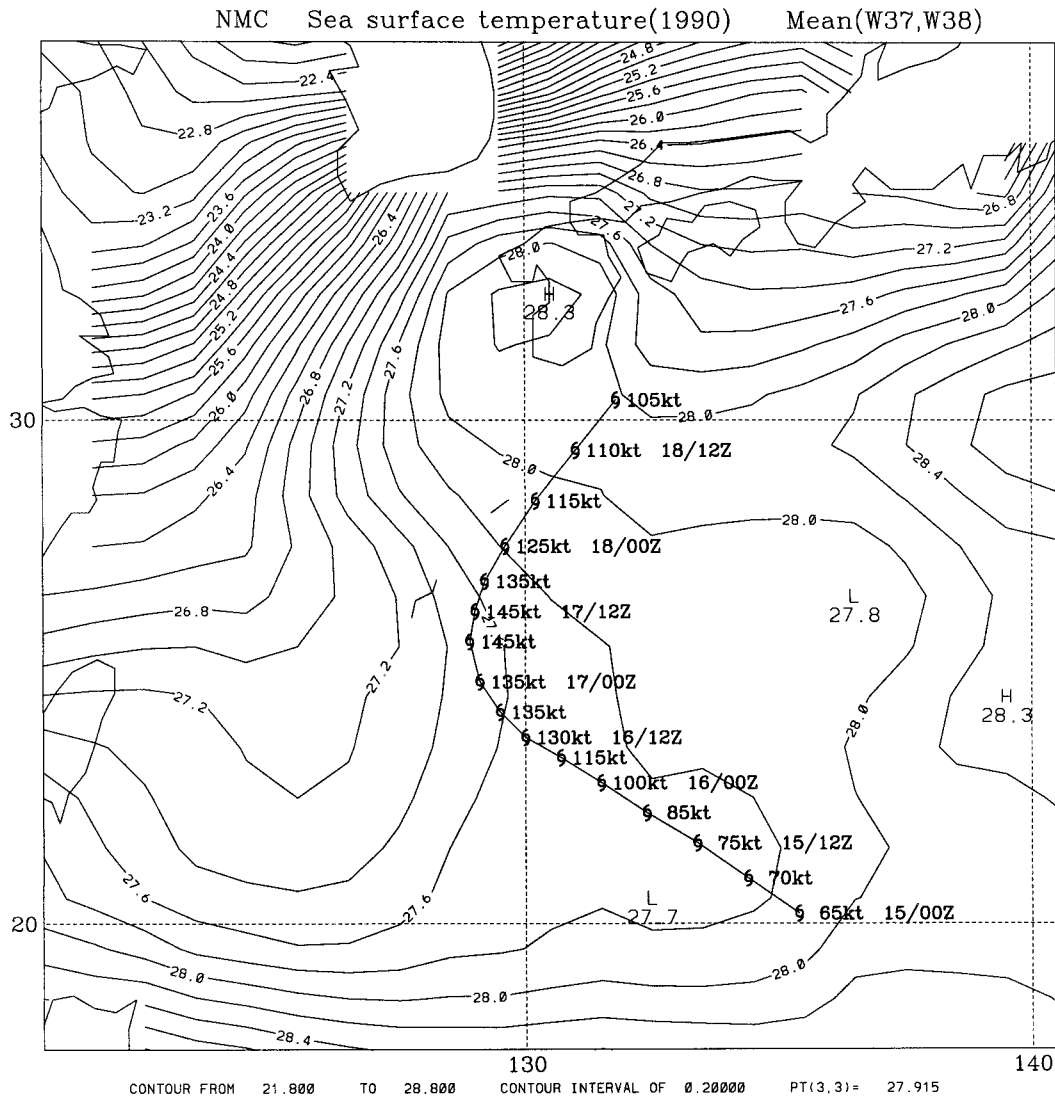


FIG. 2. NCEP weekly mean SST analyses from 15 Sep to 22 Sep and best-track positions of Flo (1990) from JTWC.

contours) are shown in Fig. 4. This figure represents a typical axisymmetric PV structure of Flo during the period of this case study, such as the maximum PV located at the lower and middle levels near the storm center, and the near-zero PV in the outflow layer (at about 345 to 370 K). Due to the coarse resolution of the global analyses, the evolution of PV in the center cannot be resolved and is not discussed here.

From 1200 UTC 15 September to 1200 UTC 17 September (Figs. 4a and 4b), the magnitude of PV outside the storm center in the outflow layer decreased with time. The largest negative PV tendency occurred on 355 K at 6° from the storm center, which is likely to be due to the low PV air carried out from the upper part of the storm center by the outflow [similar to the effect discussed in Wu and Kurihara (1996)]. In contrast to the decrease in PV in the outflow layer, the PV near the

central region kept increasing with time in both the rapid-intensification and mature stages (Figs. 4a and 4b). These results are consistent with the observation that Flo intensified during the 48-h period between 1200 UTC 15 September and 1200 UTC 17 September. As Flo's intensity started to weaken, the negative tendency of axisymmetric PV in the outflow layer is not found (Fig. 4c).

Merrill and Velden (1996) used TCM-90 (Elsberry 1990; Elsberry et al. 1990) rawinsondes and satellite cloud motion wind to show that the net outflow at 6° radius extended over an increasing θ range as Flo intensified. In this paper, the vertical structure of the radial outflow of Flo at 6° radius is also investigated based on ECMWF TOGA advanced analysis (Fig. 5). Following Merrill and Velden (1996), the *significant outflow* is also defined as the flow regime with a radial wind exceeding

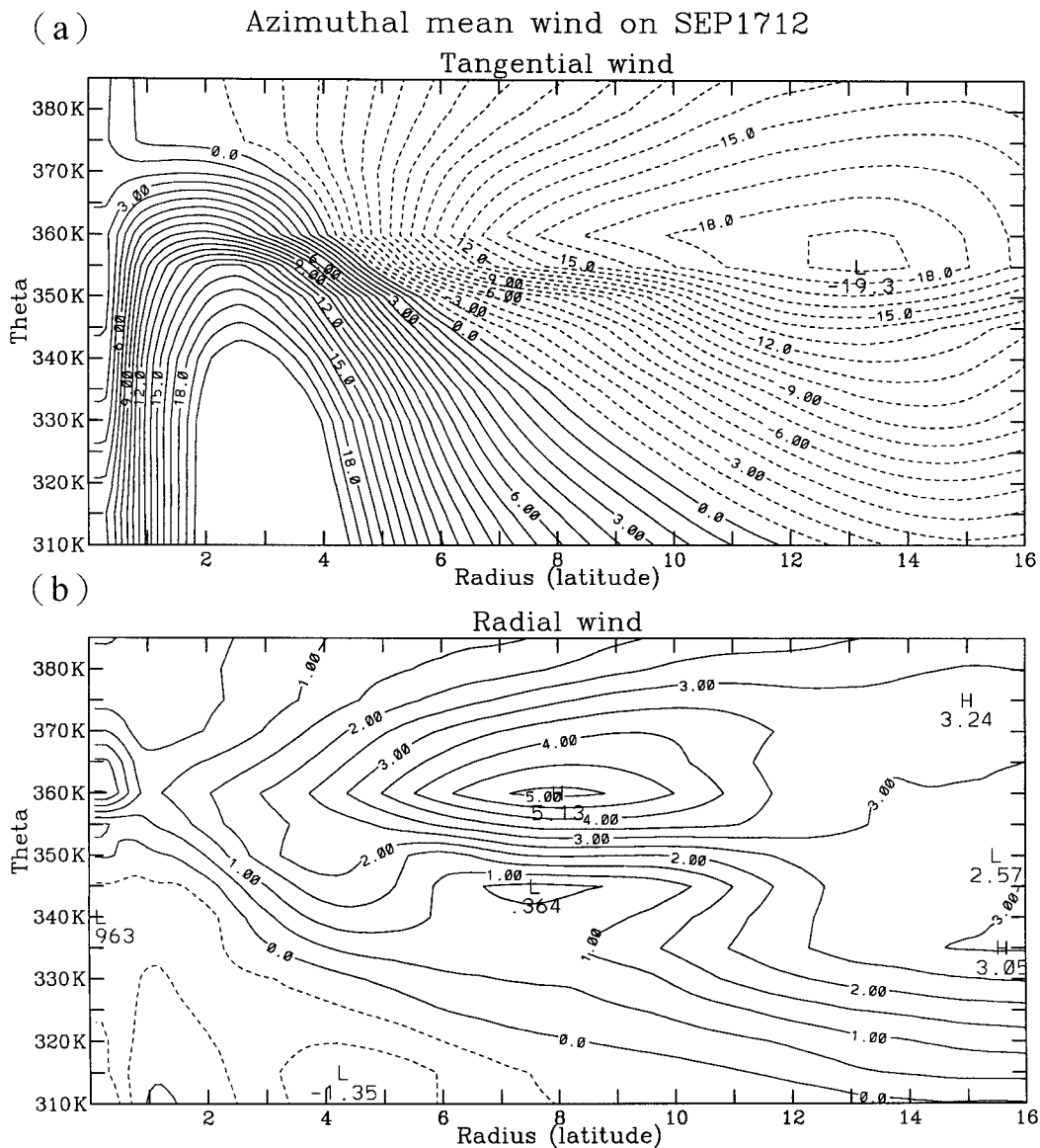
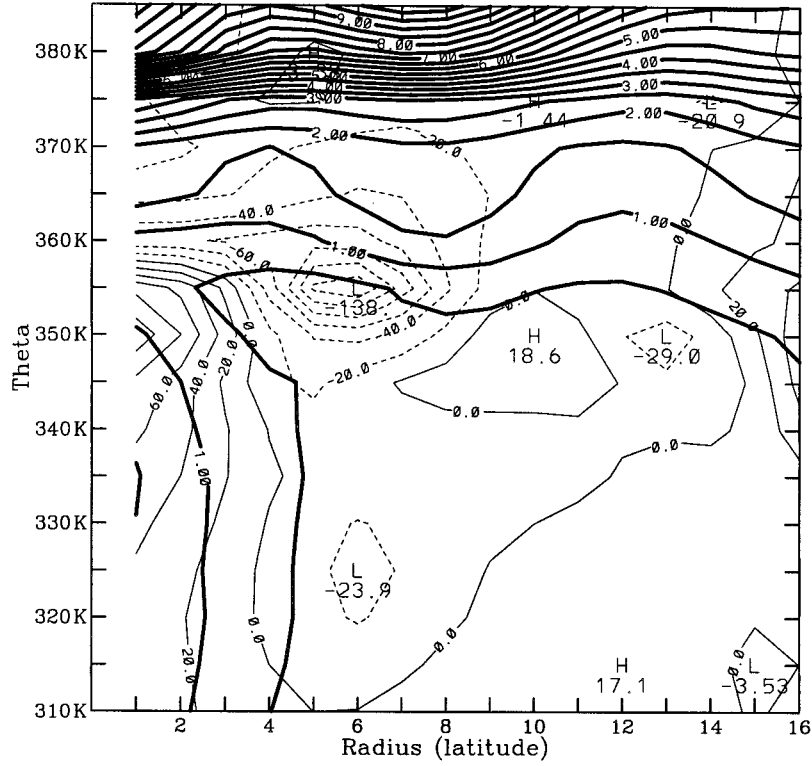


FIG. 3. Azimuthal means of ECMWF TOGA advanced analyses of (a) radial and (b) tangential winds ($m s^{-1}$) for Typhoon Flo (1990) at 1200 UTC 17 Sep.

2 $m s^{-1}$. Figure 3a shows that the lowest significant outflow is located at the 350 K θ surface during both the rapid-intensification and mature stages. The θ range associated with the outflow varies with time, and three peaks appeared separately at 1200 UTC 15 September, 0600 UTC 17 September, and 0000 UTC 18 September. Compared to the results from Merrill and Velden (1996), the radial outflow at 6° radius was poorly reproduced by ECMWF TOGA advanced analyses from 0000 UTC 16 September to 0000 UTC 17 September (Fig. 5). It appears that the cloud motion wind derived from geostationary satellite imagery, as employed in Merrill and Velden (1996), should have produced a better upper-tropospheric flow field in Flo. In addition, the

maximum low-level winds of Flo are also underestimated by the ECMWF TOGA advanced gridded analyses. The underestimation arises partly from the coarse resolution of the ECMWF analyses and the lack of observation over the ocean. Besides, the radial outflow in our analysis mostly represented the outflow associated with rotational wind of the upper-level environmental features [such as the midlatitude trough and the tropical upper-tropospheric trough (TUTT) cell] as the upper-level environmental systems are in the vicinity of Flo, whereas the radial outflow primarily represents the divergent wind of Flo when the environmental systems are at a distance. As shown in Molinari et al. (1992), the mean radial velocity of tropical cyclones are poorly

Azimuthal mean PV tendency from SEP1512 to SEP1612
(a)



Azimuthal mean PV tendency from SEP1612 to SEP1712
(b)

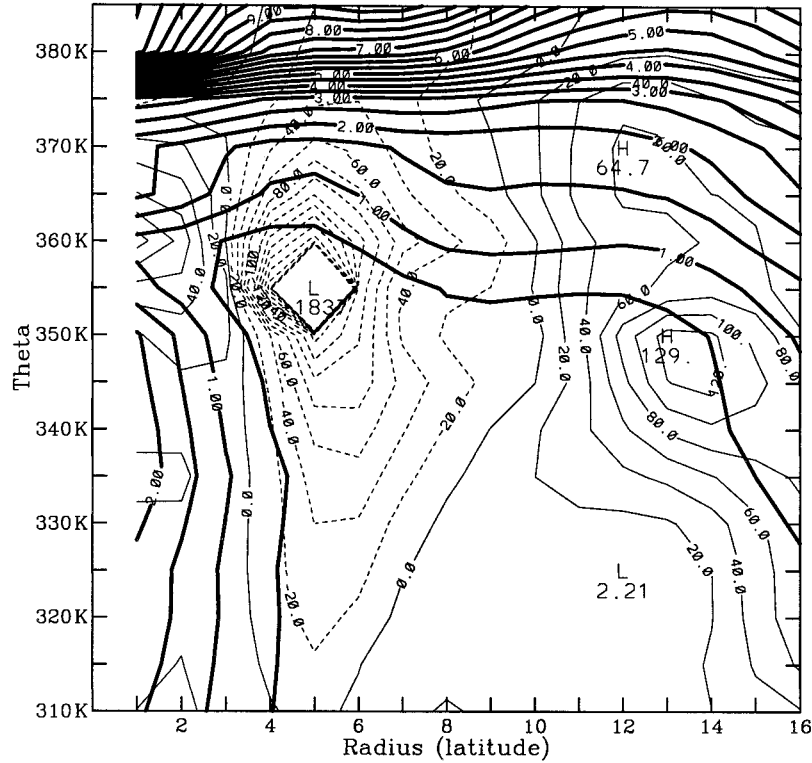


FIG. 4.

Azimuthal mean PV tendency from SEP1712 to SEP1812

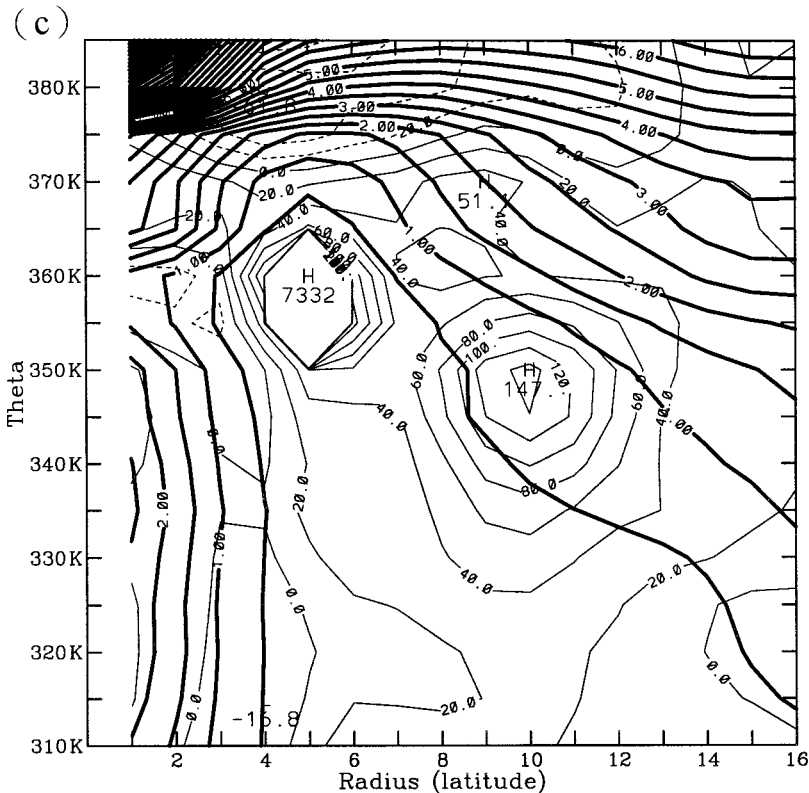


FIG. 4. (Continued) Potential temperature vs radius cross sections of the 24-h mean axisymmetric PV [bold contours; in units of $1 \times 10^{-6} \text{ m}^2 \text{ K s}^{-1} \text{ kg}^{-1}$ (1 PVU)] and the percentage change in axisymmetric PV for a 24-h period (thin contours; negative values are dashed) for Typhoon Flo (1990): (a) 1200 UTC 15 Sep–1200 UTC 16 Sep, (b) 1200 UTC 16 Sep–1200 UTC 17 Sep, (c) 1200 UTC 17 Sep–1200 UTC 18 Sep.

reproduced by the ECMWF analyses and thus the azimuthal mean radial wind of Flo was underestimated between 0000 UTC 16 September and 0000 UTC 17 September.

b. Outflow-layer analyses

The evolution of PV and wind fields is analyzed on the 355 K θ surface (Fig. 6), where the largest negative 24-h PV tendency appeared during the rapid-intensification stage. The PV at 355 K shows a low PV area over Flo and a high PV belt around the northern edge of the low PV air at 0000 UTC 15 September (figure not shown). The high PV belt extended from the TUTT cell east of Flo to the north and the west of the storm center. Two outflow jets moved along the high PV belt with an anticyclonic branch curving eastward to the TUTT and the other branch confluent with the outflow of Typhoon Ed (1990), which was southwest of Flo (Fig. 6a). As Flo intensified, the low PV area over Flo expanded, and the high PV belt was gradually eroded by the low PV air ejected from the storm center. The anticyclonic outflow jet north of the center weakened and

the westward outflow jet strengthened at 1200 UTC 16 September (Fig. 6b) after the high PV belt was cut off by the low PV air.

During the period of Flo's rapid intensification (Figs. 6a–c), the low PV area on top of Flo continued expanding. Several negative PV areas were found in the vicinity of the outflow jets. When Flo recurved northeastward, the outflow jet to the north of the storm center converged with the southwesterly wind ahead of the midlatitude trough (Fig. 6c). As the TUTT cell moved westward and got closer to Flo, an anticyclonic outflow jet originating to the south of the storm center was observed (Fig. 6d). The two outflow jets advected the low PV air from the storm center outward, and thus a northeast–southwest elongated low PV area was produced between the trough and the TUTT.

c. Eliassen–Palm flux

The E–P flux and its divergence are shown in Fig. 7a. [Note that the radial (eddy momentum flux) and vertical (eddy heat flux) components have different units. We have multiplied the heat flux term by a factor

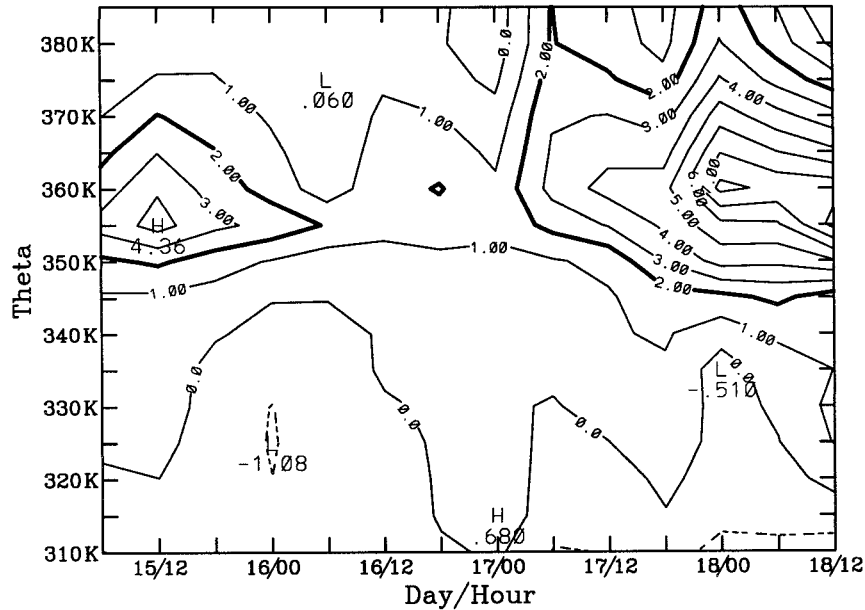
Azimuthal mean of radial wind at $R=6^\circ$ 

FIG. 5. Potential temperature vs time cross section of azimuthal-mean radial wind (m s^{-1}) at 6° lat radius. Bold line bounds region with radial wind exceeding 2 m s^{-1} .

of 10^5 to make the vertical component of the E–P flux look more distinct.] The contributions of the eddy momentum/heat flux [the first/second term on the right-hand side of Eq. (3)] to the E–P flux divergence at 1200 UTC 15 September are shown in Figs. 7b and 7c. As shown in Fig. 7a, a maximum E–P flux divergence appeared at $\sim 345\text{--}355 \text{ K}$ within a $5^\circ\text{--}8^\circ$ radius at 1200 UTC 15 September, indicating the accumulation of azimuthal mean cyclonic angular momentum. The maximum E–P flux divergence occurred at approximately the radius where there is a high PV belt north of the storm center. It is found that the eddy momentum flux term produced E–P flux divergence in the outflow layer during the rapid-intensification stage (Fig. 7b), while at the same time, the eddy heat flux term produced much weaker E–P flux convergence in the outflow layer (Fig. 7c). It is also found in Fig. 7a that the pattern of the E–P flux divergence is similar to that associated with the eddy momentum flux (Fig. 7b). In other words, the eddy heat fluxes make a very minor contribution to the E–P flux divergence.

In the mature stage, the divergence of the E–P flux within a 10° radius was still dominated by the eddy momentum flux term, but the effect of eddy heat fluxes became more important in the decaying stage (figures

not shown). Moreover, in the last two stages, the eddy momentum flux and the eddy heat flux both produced divergence of the E–P flux in the outflow layer.

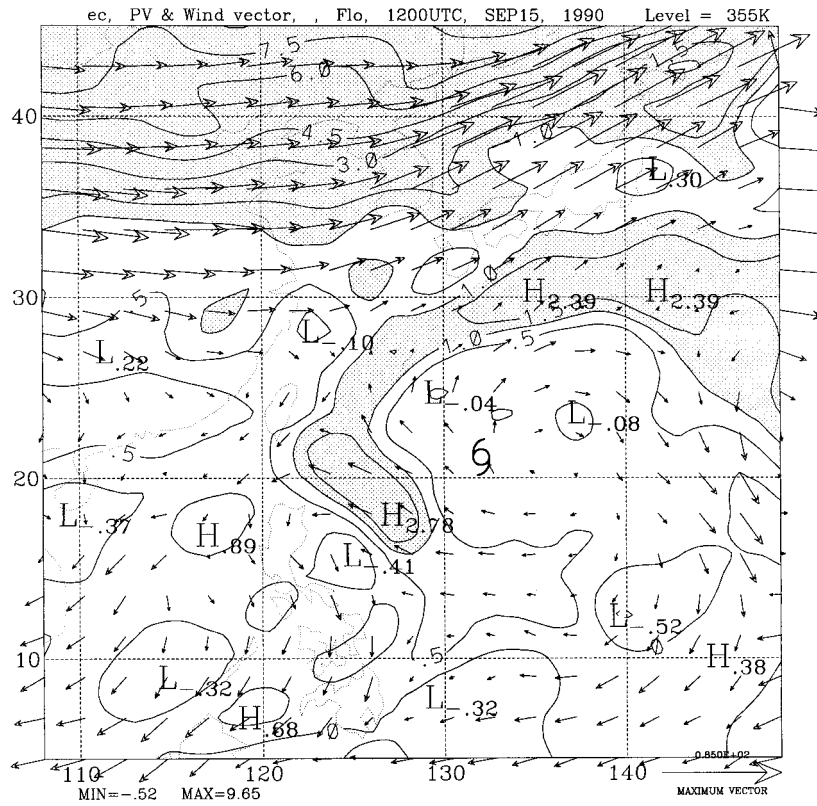
d. Eddy flux convergence of relative angular momentum

Figure 8 shows that a maximum EFC occurred at a 5° radius at 1200 UTC 15 September, and at the same time, the azimuthal mean radial outflow at 200 hPa strengthened (Fig. 9). The maximum EFC shifted outward with time in the rapid-intensification stage. At 1800 UTC 15 September, the 400-hPa azimuthal mean radial inflow (not shown) occurred, and remained during the rapid intensification stage, weakening in the mature stage. The radial outflow at 200 hPa decreased between 0000 UTC 16 September and 0000 UTC 17 September (Fig. 9), when the minimum EFC appeared at 200 hPa (Fig. 8).

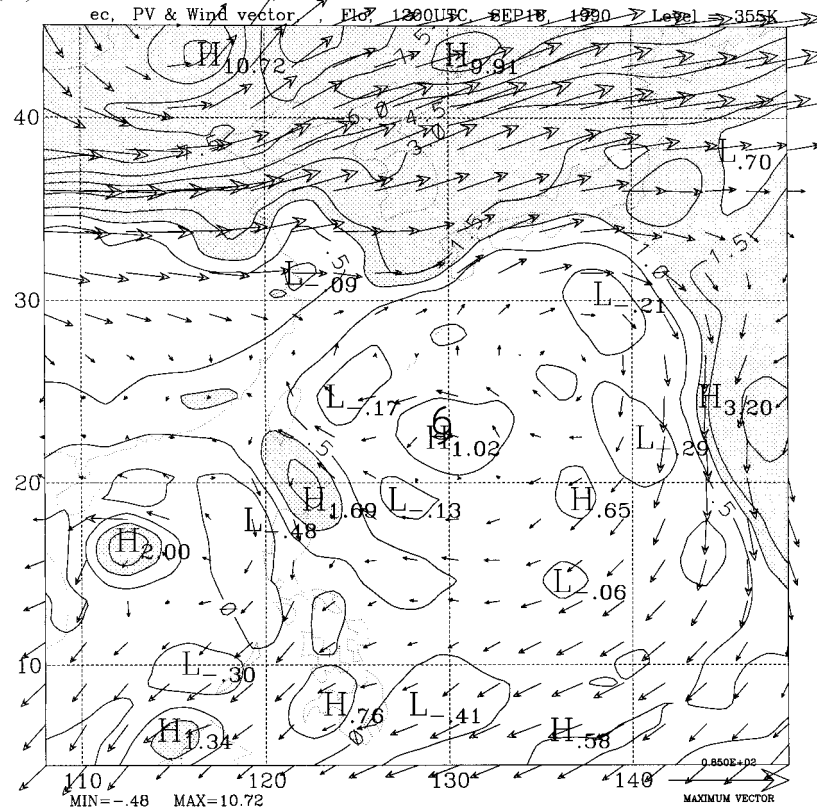
The positive EFC reappeared within a 10° radius at 0600 UTC 17 September, and increased in the decaying stage (Fig. 8). The increase of EFC was accompanied with the strengthening of the 200-hPa radial outflow, and the weakening of the 200-hPa cyclonic wind (Fig. 9).

FIG. 6. Wind vectors and PV on the 355 K isentropic surface at (a) 1200 UTC 15 Sep, (b) 1200 UTC 16 Sep, (c) 1200 UTC 17 Sep, and (d) 1200 UTC 18 Sep. PV values greater (smaller) than $1.5 \times 10^{-6} \text{ m}^2 \text{ K s}^{-1} \text{ kg}^{-1}$ (1.5 PVU) are contoured in 1.5 PVU (0.5 PVU) increments, and values greater than 1 PVU are shaded. The location of Typhoon Flo (1990) is indicated by the tropical cyclone symbol.

(a)



(b)



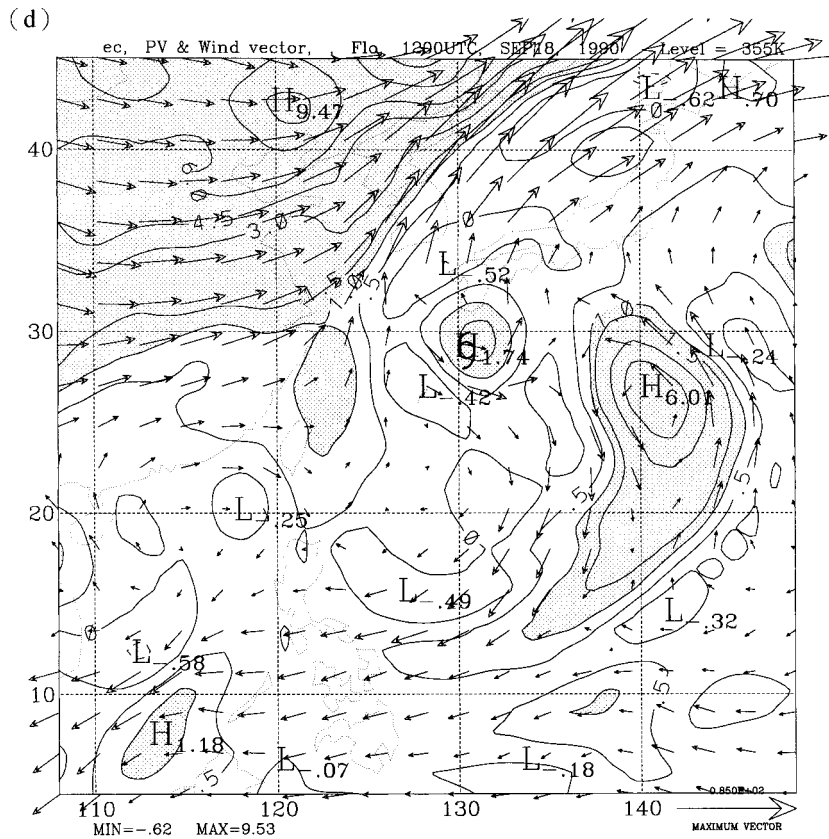
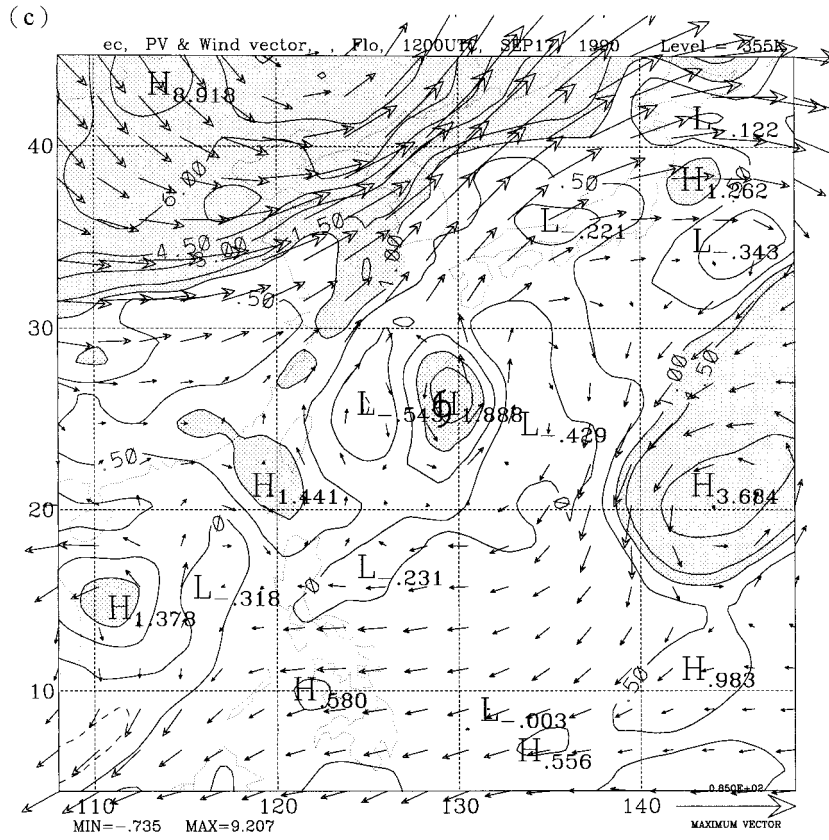


FIG. 6. (Continued)

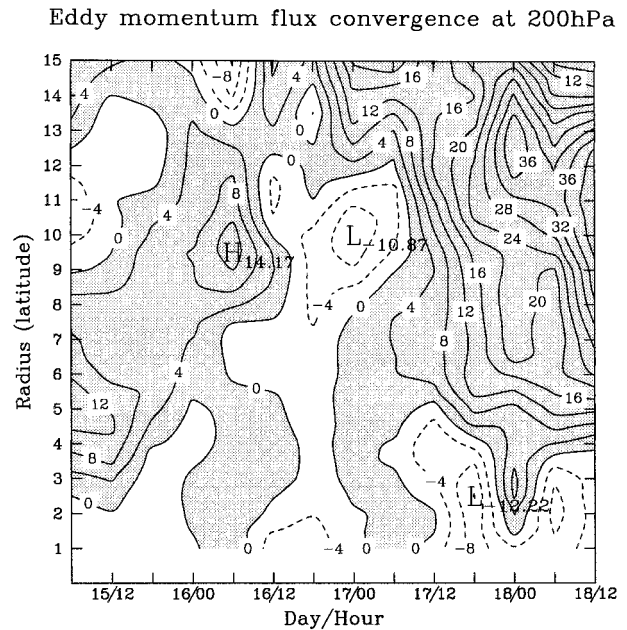
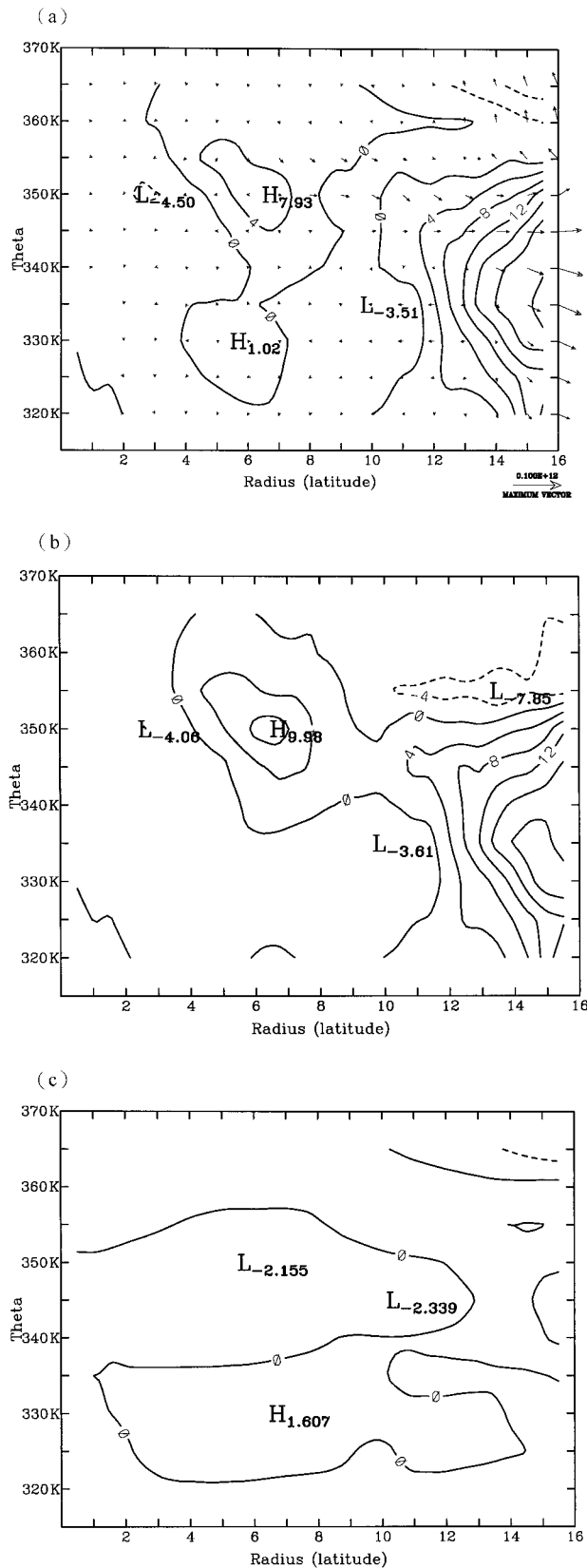


FIG. 8. Time series of EFC of angular momentum at each radius at 200 hPa for Typhoon Flo (1990). Contour interval is $4 \text{ m s}^{-1} \text{ day}^{-1}$. Negative values are dashed; positive values are shaded.

Obviously, the enhancement of EFC does not guarantee intensification of a typhoon.

e. The effect of vertical wind shear

The vertical wind shears derived from both the A method and the K method (see section 2b.4 for definition), and the maximum surface wind from JTWC are shown in Fig. 10a. The result shows that both shears are comparable at time periods before Flo reached its maximum intensity at 1200 UTC 17 September. Meanwhile, as shown in Fig. 10b, the distribution of horizontal wind at all levels clearly indicates the reliability in the definition of the vertical wind shear. It is found from Fig. 10 that Flo's intensification rate increased as the vertical shear decreased at 1800 UTC 15 September. The vertical shear stayed below 4 m s^{-1} in both the rapid-intensification and mature stages. The increase in the vertical wind shear started at 1200 UTC 17 September and continued for 6 h. Then, after a temporary decrease, the vertical wind shear increased rapidly.

FIG. 7. (a) Potential temperature vs radius cross sections of E-P flux vectors and their divergence at 1200 UTC 15 Sep 1990. The vertical component (eddy heat flux) of the E-P flux is scaled by 5×10^4 . (b) Contribution of eddy momentum flux to E-P flux divergence at 1200 UTC 15 Sep 1990. Contour interval is $4 \times 10^4 \text{ Pa m}^2 \text{ K}^{-1} \text{ s}^{-2}$, and negative values are dashed.

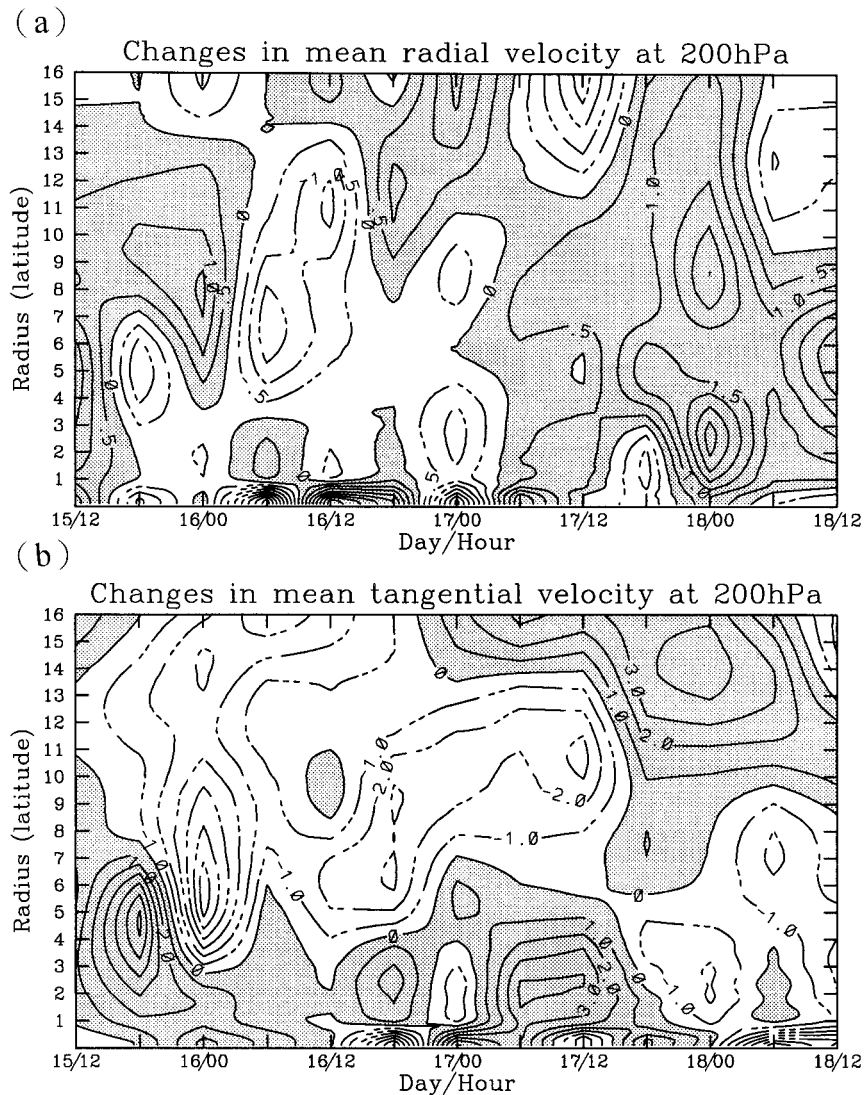


FIG. 9. Changes in azimuthal mean winds for Typhoon Flo (1990) at 200 hPa for 6 h ending at time shown: (a) radial wind (contour interval of 0.5 m s^{-1}) and (b) tangential wind (contour interval of 1 m s^{-1}). Positive values are shaded; negative values are dashed.

4. Typhoon Gene

The initial disturbance resulting in Gene was formed west-southwest of Guam and for 5 days, the maximum wind was less than 13 m s^{-1} (Rudolph and Guard 1990). Gene became a typhoon at 1800 UTC 25 September 1990. As shown in Fig. 11, Gene started to intensify again after 0000 UTC 26 September, reaching peak intensity with a maximum surface wind of 80 kt at 1800 UTC 26 September. The peak intensity was maintained for 60 h, and then Gene weakened slowly. Gene initially moved along the equatorward side of the midlevel subtropical ridge, and then turned northwestward (Fig. 11). After curving to the west of Okinawa, Gene accelerated east-northeastward and became an extratropical low to the east of Tokyo on 30 September.

Following section 3, three periods between 1800 UTC 25 September and 0600 UTC 30 September are identified: 1) the intensifying stage, from 1800 UTC 25 September to 1800 UTC 26 September; 2) the steady stage, from 1800 UTC 26 September to 0600 UTC 29 September; and 3) the decaying stage, from 0600 UTC 29 September to 0600 UTC 30 September. The discussion in this section is focused on Gene's evolution in the intensifying stage.

a. Axisymmetric structure

Figure 12 shows the r - θ cross section of 24-h mean axisymmetric PV (bold solid contours) and the rate of axisymmetric PV change in a 24-h period (thin con-

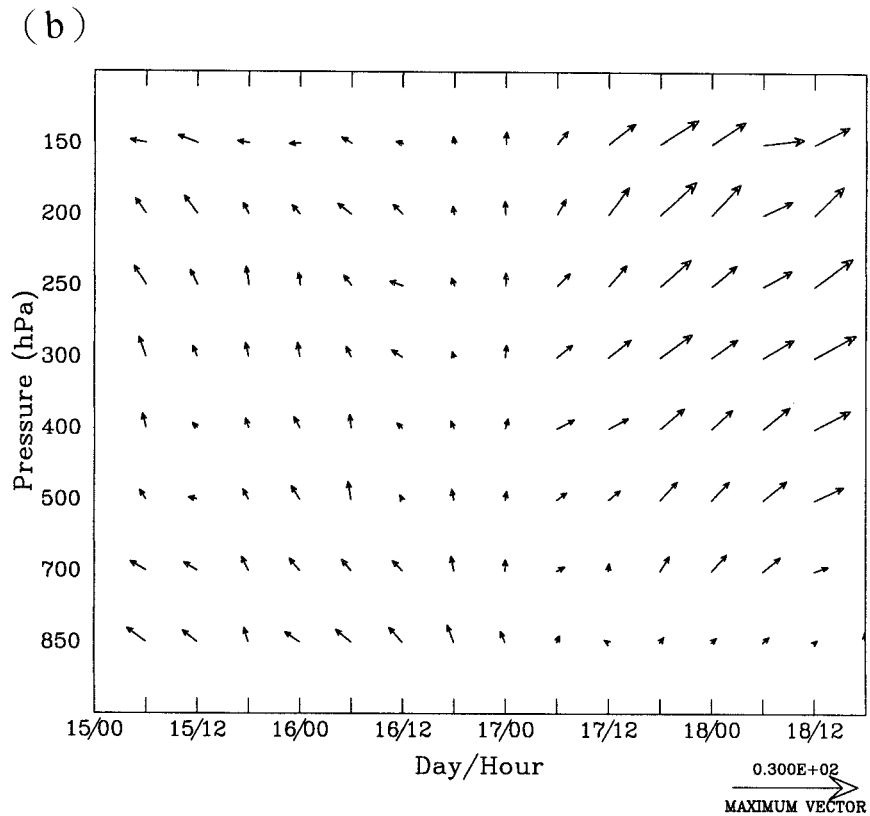
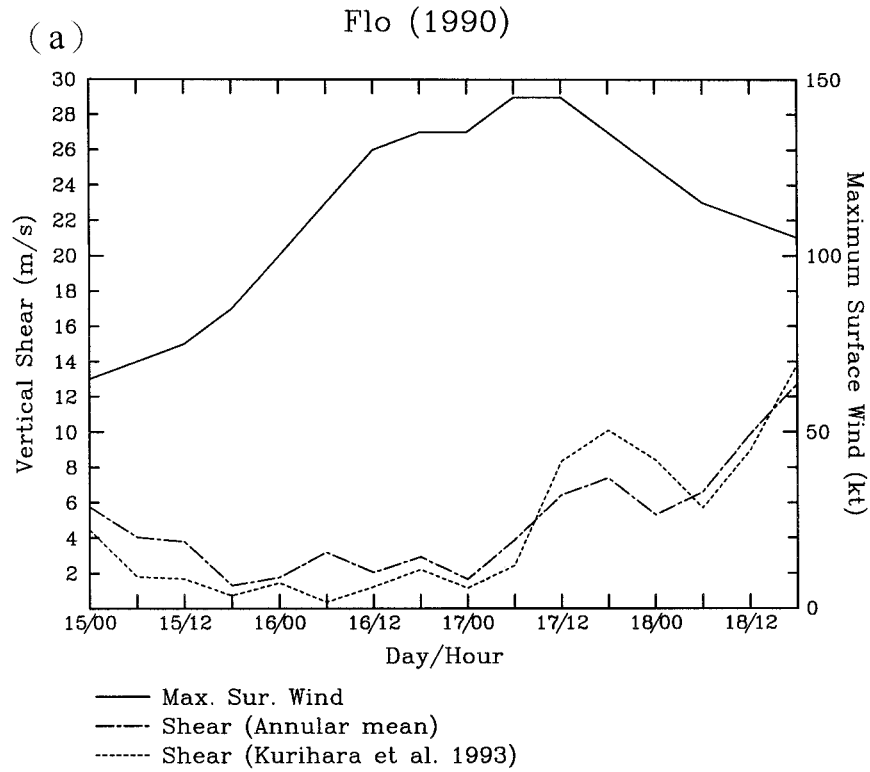


FIG. 10. (a) Time variation of vertical wind shear obtained from A method (dash-dot) and K method (small dashes) and maximum surface wind (solid) from JTWC for Typhoon Flo (1990). (b) Time variation of vertical wind shear vectors at the storm center obtained from K method for Typhoon Flo (1990).

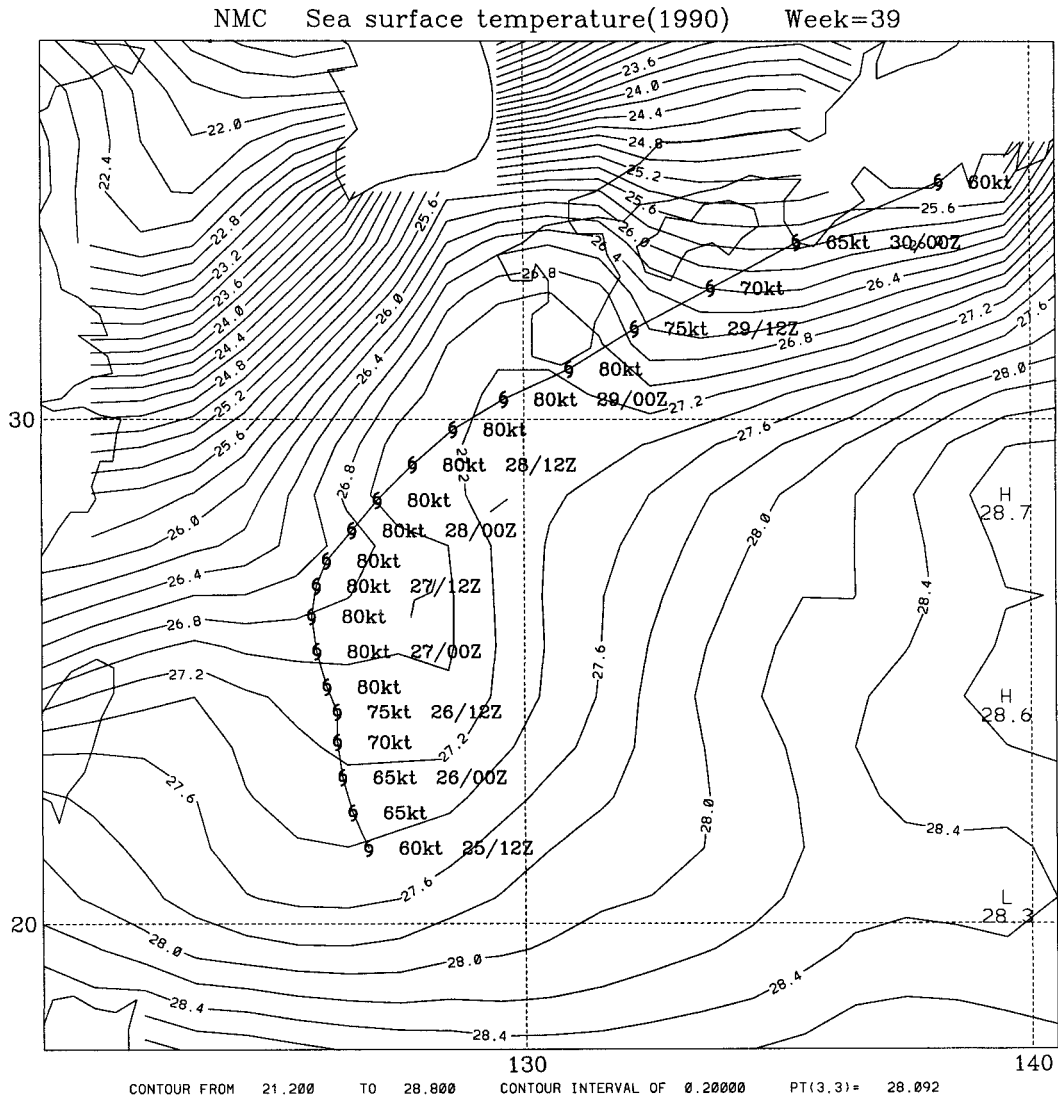


FIG. 11. NCEP weekly mean SST analyses from 23 Sep to 29 Sep and best-track positions of Gene (1990) from JTWC.

tours). In the 24 h before 0000 UTC 27 September (Fig. 12a), during which Gene intensified steadily, the axisymmetric PV increased near the storm center in the lower layer and decreased in the outflow layer. The largest negative PV tendency occurred at 345 K at a radius of about 8° from the center. In the steady stage (Fig. 12b), the decrease in axisymmetric PV in the outflow layer was not as apparent as in the intensifying stage, and the axisymmetric PV near the storm center did not increase again. Instead, Fig. 12b shows that the upper-level axisymmetric PV increased outside the 8° radius, and the region with maximum positive PV tendency shifted inward with time (figures not shown). The in-

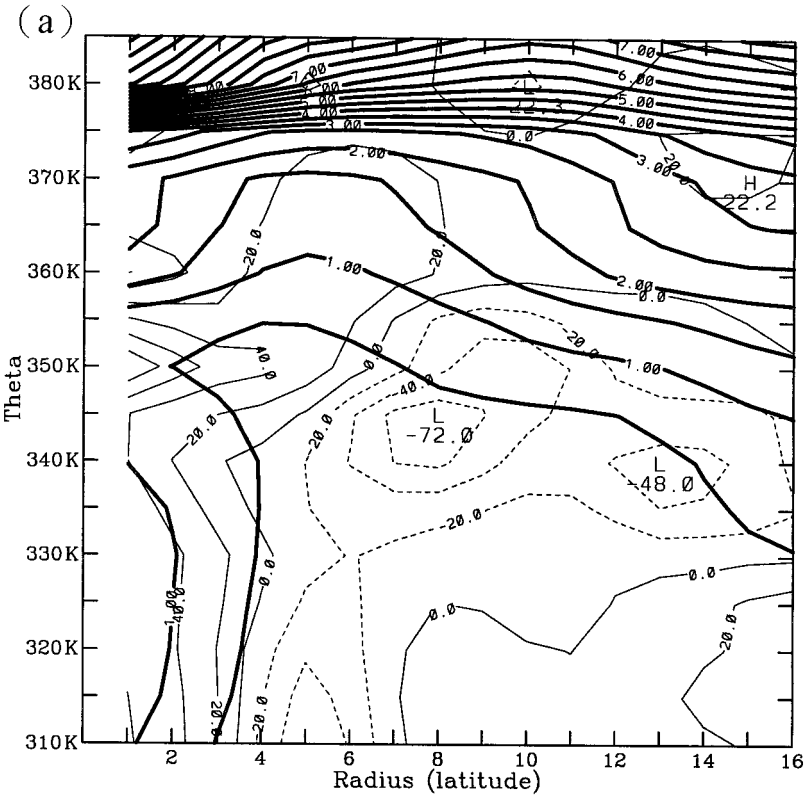
ward shifting of the maximum positive axisymmetric PV tendency was associated with the approaching of an upper-level positive PV anomaly.

The azimuthal mean wind at 0000 UTC 27 September, when Gene reached its peak intensity, is shown in Fig. 13. Figure 13a shows that the maximum tangential wind in the gridded analyses is located at a 2.5° radius, and that the maximum radial outflow occurs at a 4° radius at 350 K. The low-level inflow is located under 315 K (Fig. 13b), and a secondary inflow appeared at 340 K.

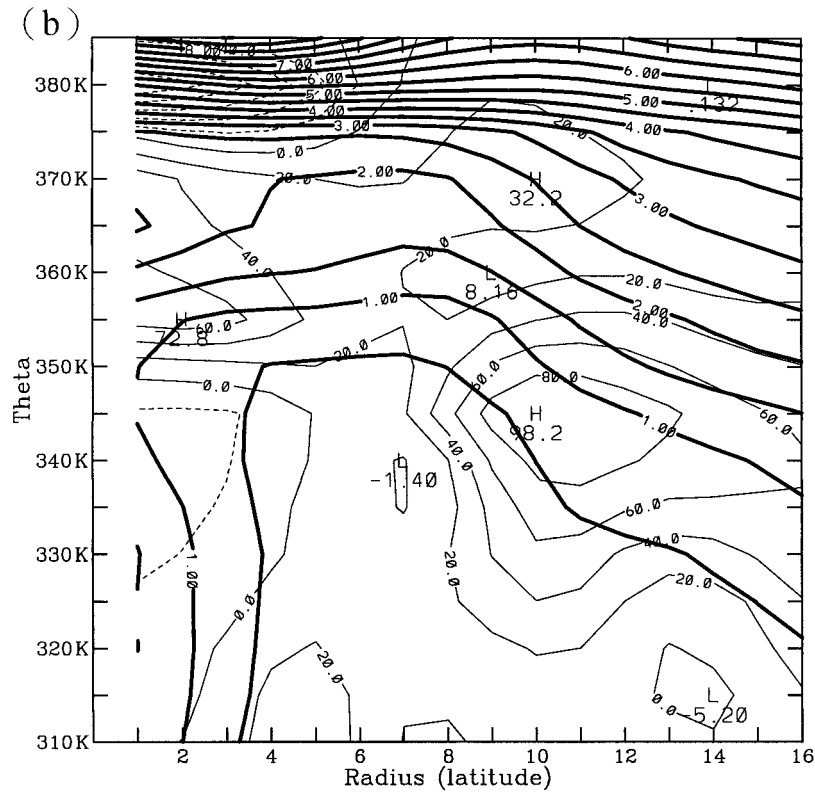
The evolution of the vertical extent of the azimuthal-mean radial wind on the isentropic coordinate is analyzed at a 4° radius (Fig. 14), which is the radius of the

FIG. 12. As in Fig. 4 but for Typhoon Gene (1990): (a) 0000 UTC 25 Sep–0000 UTC 26 Sep, (b) 0000 UTC 26 Sep–0000 UTC 27 Sep.

Azimuthal mean PV tendency from SEP2600 to SEP2700



Azimuthal mean PV tendency from SEP2700 to SEP2800



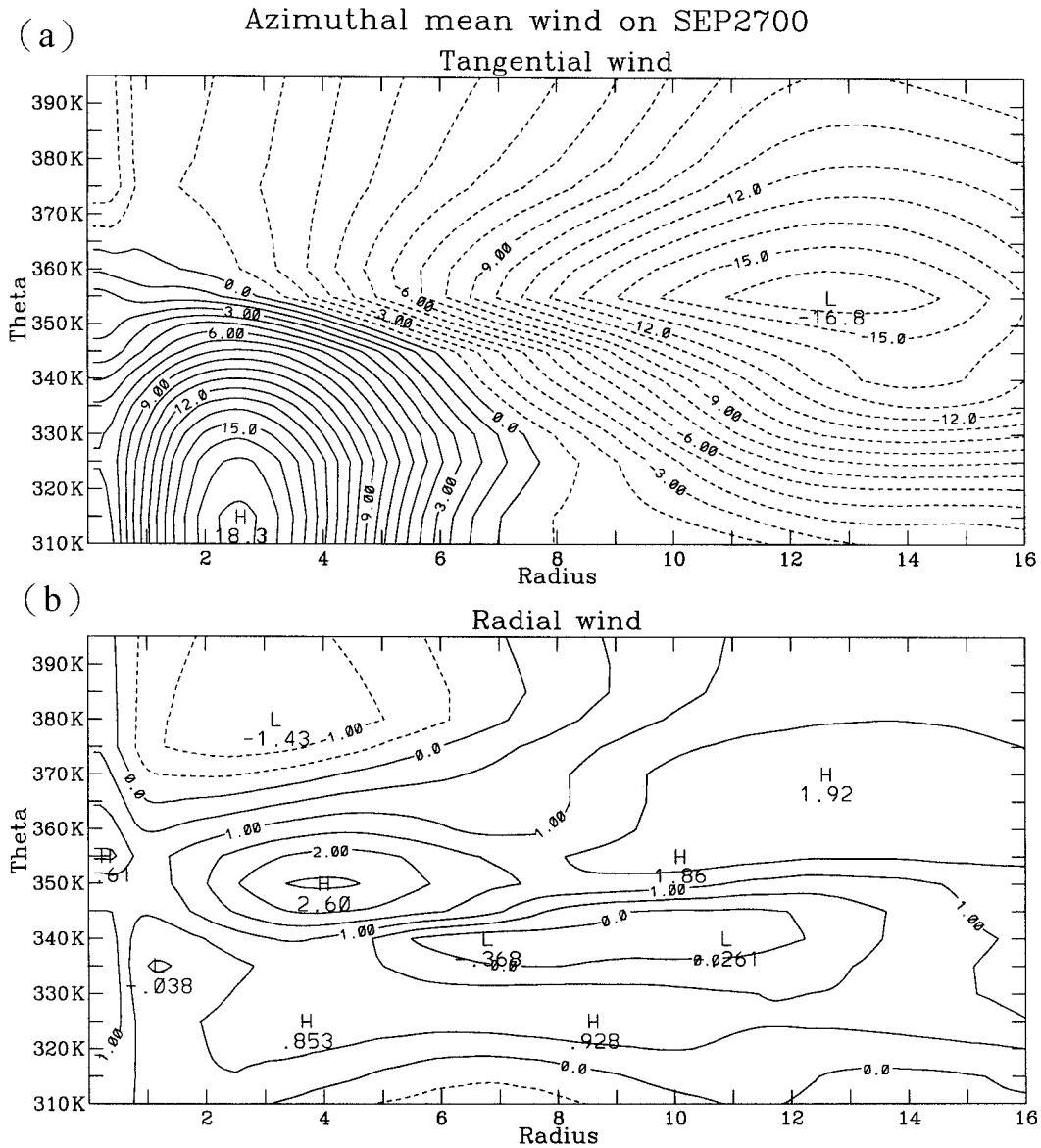


FIG. 13. As in Fig. 3 but for Typhoon Gene (1990) at 0000 UTC 27 Sep.

maximum radial outflow during Gene's peak intensity. The θ range of the significant outflow is not evident until Gene reached its peak intensity. In the steady stage, the vertical extent of the radial outflow at a 4° radius generally ranged from 340 to 360 K. Compared with Typhoon Flo, the vertical extent of Gene's outflow on the isentropic coordinate is smaller. While the ECMWF TOGA advanced analyses generally reproduced the tendency but underestimated the magnitude of the intensity during Gene's intensification stage, the analysis data did not capture the decay.

b. Outflow-layer analyses

The maximum outflow during Gene's peak intensity is located at the 350 K θ surface, therefore the evolution

of the PV and wind fields is analyzed at 350 K (Fig. 15). Figure 15a shows a low-PV region over Gene. An area with positive PV associated with a TUTT cell was located to the east of Gene. An anticyclonic outflow jet originating from the north of the storm center curved around the western edge of the TUTT (Fig. 15a). Another high-PV feature associated with a midlatitude trough to the northwest of Gene was moving eastward. The outflow jet to the northeast of the storm center was confluent with the strong westerly winds ahead of the trough (Fig. 15a). As the center of the trough passed to the north of Gene's center, a high-PV strip extended from the base of the trough to the northwest of Gene (Fig. 15b). The intensification of Gene stopped when the high-PV strip separated from the moving trough

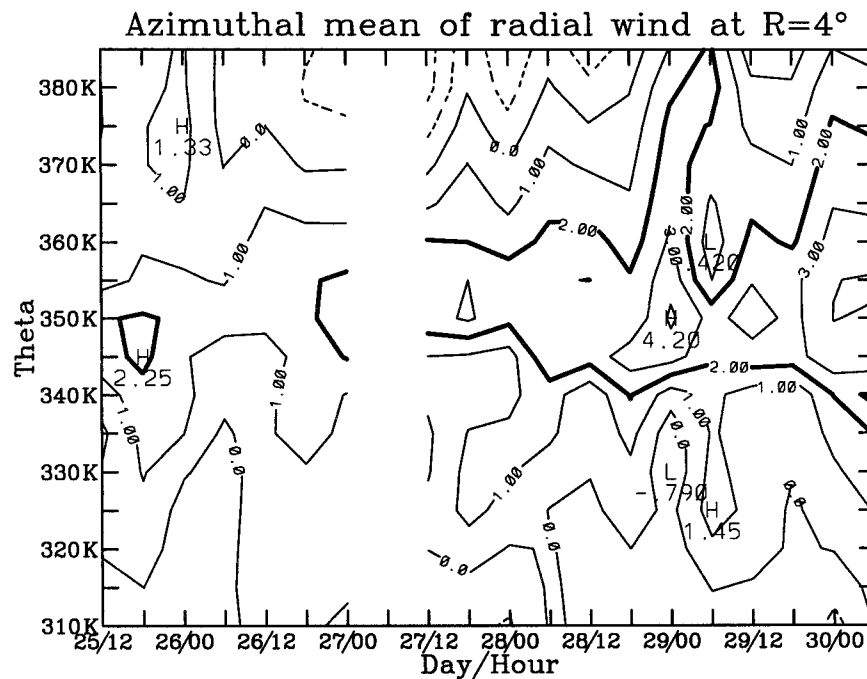


FIG. 14. (a) Potential temperature vs time cross section of azimuthal mean radial wind at 4° lat radius (solid line).

(Fig. 15c). At the same time, the anticyclonic outflow jet to the northeast of the storm center strengthened, and a broad negative PV area appeared to the east of the storm center. The negative PV area is located at the downshear side of the 850–200-hPa vertical wind shear, indicating that the upper negative PV anomaly was advected to the downshear side of the lower positive PV anomaly. This is consistent with the effect of the vertical shear discussed in Wu and Emanuel (1993).

Gene moved northeastward and got closer to the strong westerly winds in the steady stage (Figs. 15d and 15e). Again, a high-PV strip extended southward from the northern positive PV anomaly at 1200 UTC 28 September (Fig. 15f). The anticyclonic outflow jet to the north of the storm center was enhanced (Fig. 15f), while the outflow to the west of the storm center was restricted by the strong westerly winds. Gene started to decay at 0600 UTC 29 September, when the high-PV strip separated from the northern positive PV anomaly.

c. Eliassen–Palm flux

The E–P flux vector and the divergence of E–P flux are shown in Fig. 16. An E–P flux divergence maximum occurred in the outflow layer as a midlatitude trough approached Gene, indicating that the mean cyclonic an-

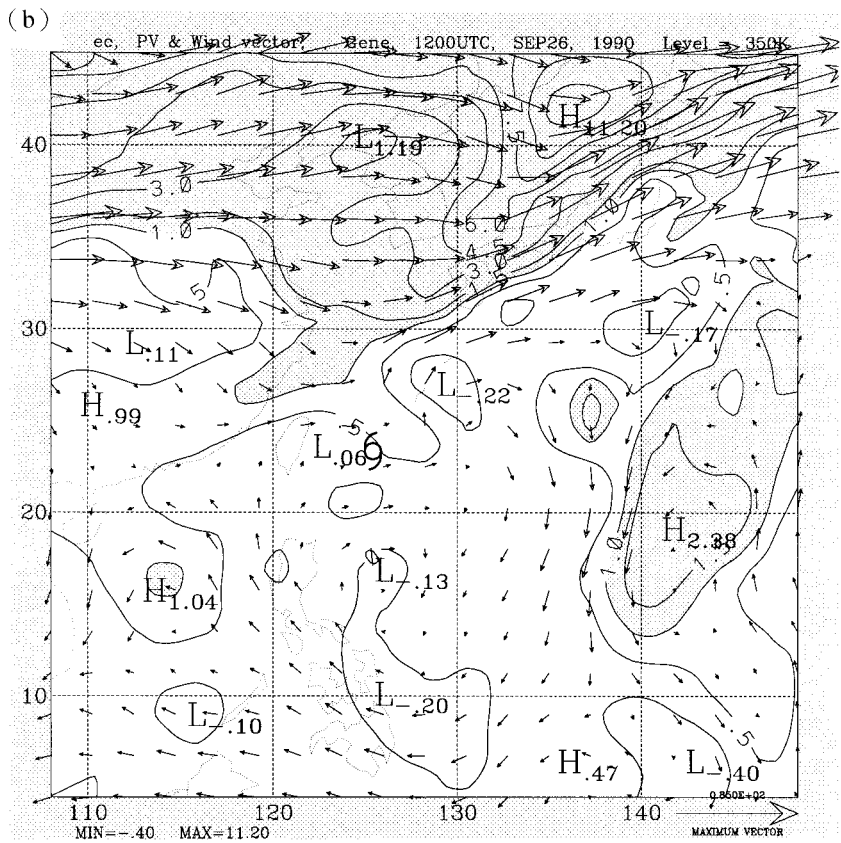
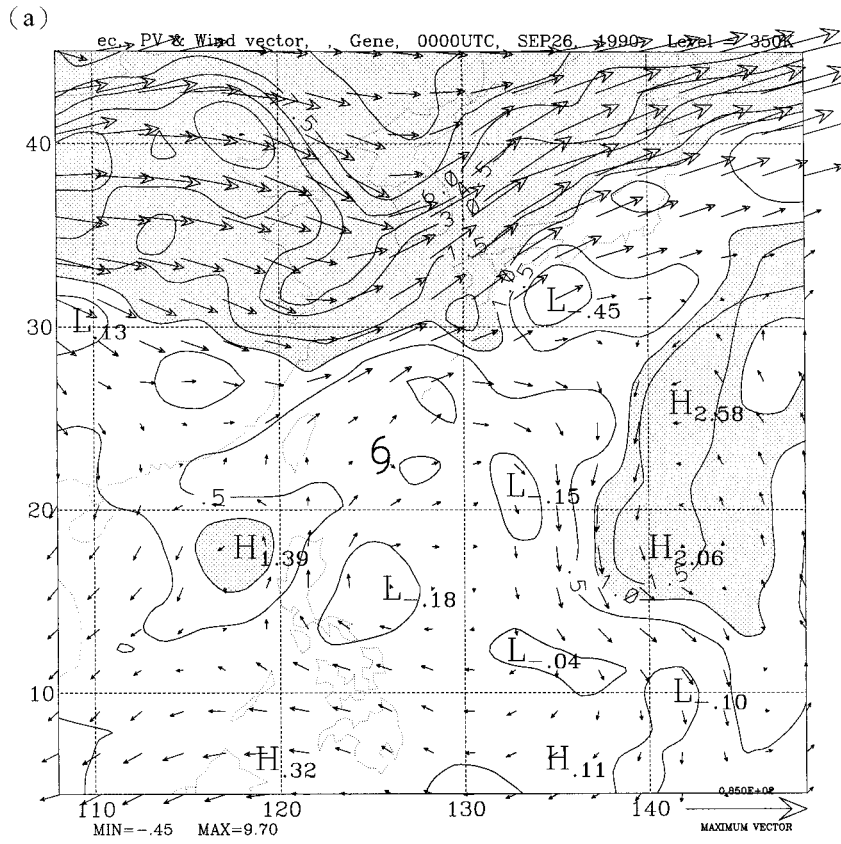
gular momentum is produced in the outflow layer. The E–P flux divergence maximum shifted into a 5° radius (Fig. 16a) when the trough was due north of Gene. In the intensifying stage, the E–P flux divergence is dominated by the eddy momentum flux term [the first term on the right-hand side of Eq. (3), Fig. 16b]. After the trough moved over the north of the storm center, the magnitude of the maximum E–P flux divergence decreased (not shown).

In the decaying stage, the positive E–P flux divergence occurred above 345 K, while the negative E–P flux divergence appeared below 345 K (Fig. 17a). As a result, the E–P flux produced an anticyclonic mean angular momentum inside the storm. During this time, the E–P flux divergence is dominated by the effect of the eddy heat flux term [the second term in the right-hand side of Eq. (3); Fig. 17b].

d. Eddy flux convergence of relative angular momentum

Figure 18 shows the evolution of EFC at 200 hPa during the 5-day period (from 1200 UTC 25 September to 0600 UTC 30 September) of this case study. The maximum EFC occurred as a midlatitude trough approached Gene. During the period of the interaction

FIG. 15. As in Fig. 6 but for Typhoon Gene (1990) on the 350 K isentropic surface at (a) 0000 UTC 26 Sep, (b) 1200 UTC 26 Sep, (c) 0000 UTC 27 Sep, (d) 1200 UTC 27 Sep, (e) 0000 UTC 28 Sep, (f) 1200 UTC 28 Sep.



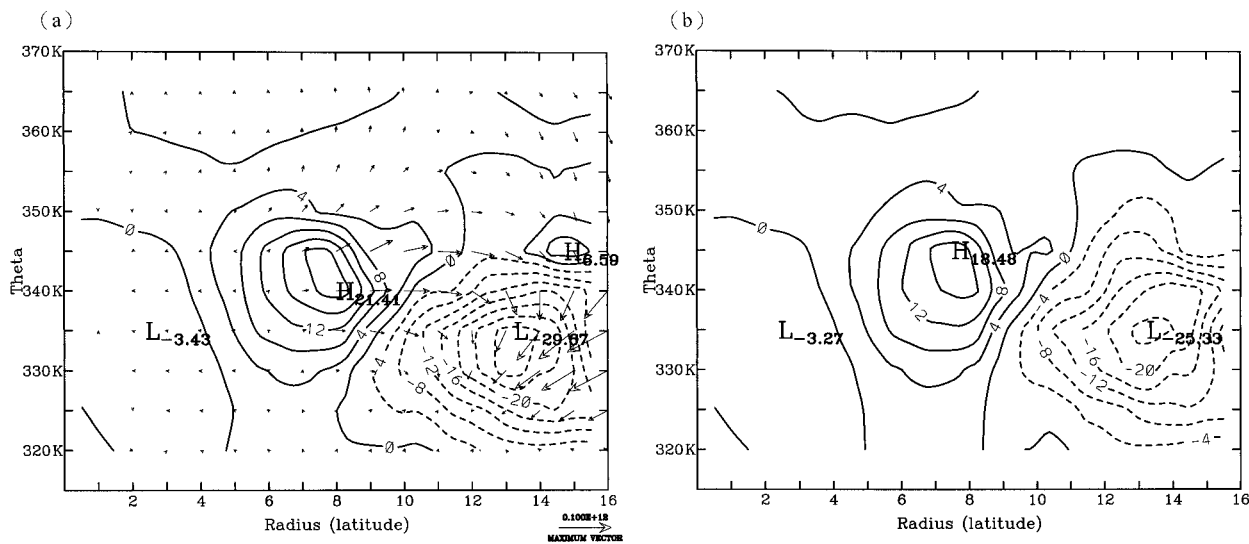


FIG. 16. (a) Potential temperature vs radius cross sections E-P flux vectors and their divergence at 0000 UTC 26 Sep 1990. The vertical component (eddy heat flux) of the E-P flux is scaled by 5×10^4 . (b) Contribution of eddy momentum flux to E-P flux divergence at 0000 UTC 26 Sep 1990. Contour interval is $4 \times 10^4 \text{ Pa m}^2 \text{ K}^{-1} \text{ s}^{-2}$ and negative values are dashed.

between Gene and the trough, the maximum EFC shifted inward with time. Gene began to intensify as the maximum EFC shifted into the vicinity of Gene's center at 0000 UTC 26 September. The azimuthal mean wind at 200 hPa shows that the radial outflow increased (Fig. 19a) and the cyclonic tangential wind was spun up (Fig. 19b) in the intensifying stage, during the period of enhanced EFC. When the EFC moved into the central region (Fig. 18), the intensification of Gene ceased. During the steady stage, another EFC maximum occurred outside a 10° radius and shifted inward with time (Fig. 18). At the same time, the cyclonic component of the

200-hPa outflow increased and the radius of maximum velocity change shifted inward with time (Fig. 19b). In the last stage, the positive EFC remained at 200 hPa (Fig. 18) and the 200-hPa radial outflow also strengthened (Fig. 19a), while the intensity of Gene decreased.

e. Vertical wind shear

The vertical wind shears derived from the A method and the K method during the period of Gene's evolution are shown in Fig. 20a. The magnitude of the vertical wind shear is greater than 10 m s^{-1} during all three

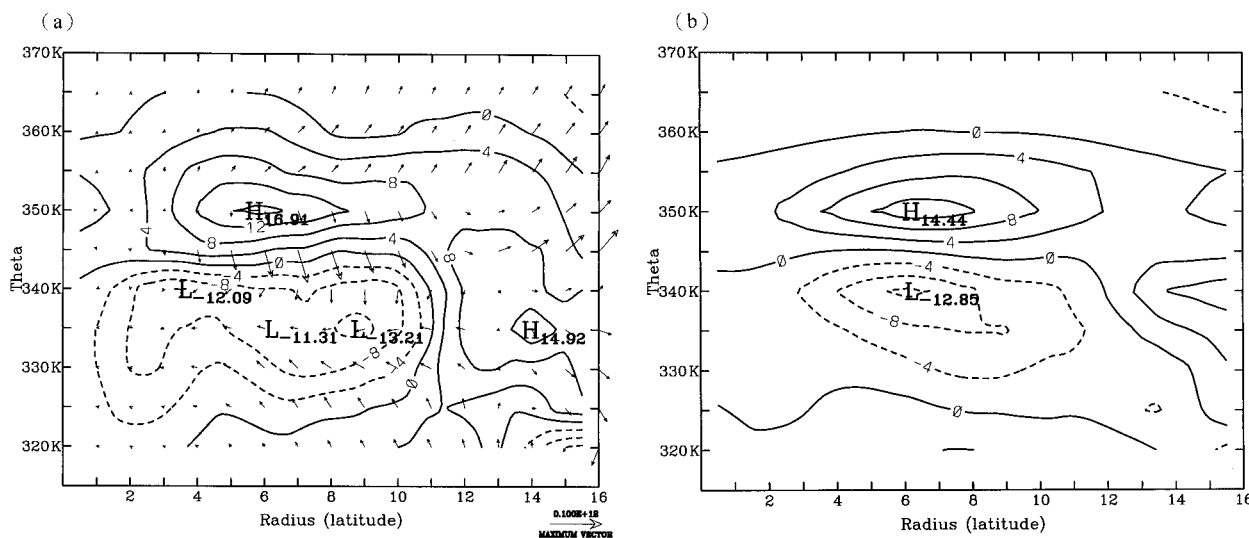


FIG. 17. (a) Potential temperature vs radius cross sections of E-P flux vectors and their divergence at 0000 UTC 29 Sep 1990. The vertical component (eddy heat flux) of the E-P flux is scaled by 5×10^4 . (b) Contribution of eddy heat flux E-P flux divergence at 0000 UTC 29 Sep 1990. Contour interval is $4 \times 10^4 \text{ Pa m}^2 \text{ K}^{-1} \text{ s}^{-2}$, and negative values are dashed.

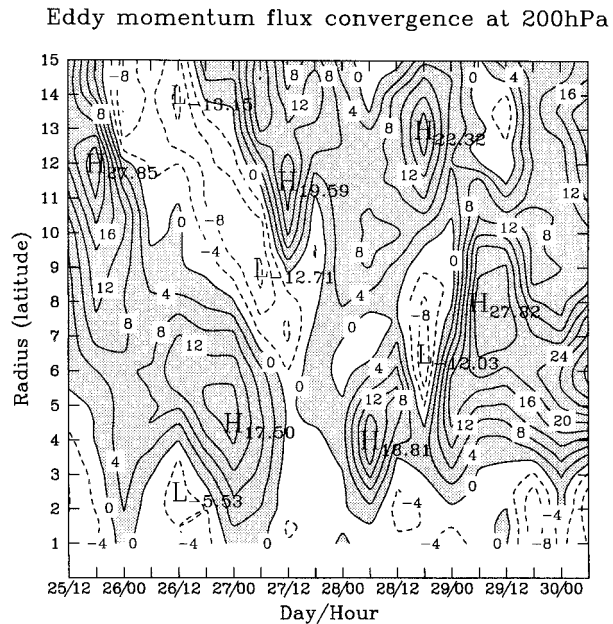


FIG. 18. As in Fig. 8 but for Typhoon Gene (1990).

stages. This large vertical shear is manifest in Fig. 20b. The vertical wind shear increased as the midlatitude trough approached; while during the interaction period between the trough and Gene, the vertical wind shear did not increase again. After the intensification of Gene stopped, the vertical shear increased slightly at 1200 UTC 27 September. The increase of the vertical shear was associated with Gene's approaching the midlatitude westerlies. Despite the increase of the vertical wind shear, the intensity of Gene did not change.

5. Discussion

The above case studies show two different developing processes for Typhoons Flo and Gene. The stronger one, Supertyphoon Flo, experienced a rapid intensification and rapid decay during a 4-day period. The weaker one, Typhoon Gene, did not intensify as rapidly as Flo, but maintained its peak intensity for about 60 h. In this section, the mechanism for the intensification of each typhoon is investigated based on the results of the case studies. Both the similarities and differences between the two cases are also discussed to understand how each mechanism, such as the eddy momentum flux, eddy heat flux, and the vertical wind shear, affected the development of Flo and Gene.

a. The intensification of supertyphoon Flo

After reaching typhoon strength, Flo continued deepening steadily. More rapid intensification of Flo occurred as the outflow was enhanced at 1200 UTC 15 September. The evolution of PV and wind fields in the outflow layer shows that the TUTT cell to the east of

Flo provided an effective channel for the outflow air. The calculation of the E-P flux and the EFC show that the eddy momentum flux produced azimuthal mean cyclonic angular momentum in the outflow layer. In addition, the evolution of the azimuthal-mean wind also shows an increase in the cyclonic component at 200 hPa during the period of the enhanced EFC.

The piecewise PV inversion (Wu and Emanuel 1995) was performed to evaluate the influence from the upper-tropospheric PV belt extended from the TUTT to the north of Flo. The balanced flow associated with this upper PV anomaly produced a weak cyclonic circulation (figures not shown) centered near Flo at the lower levels. The amplitude of this balanced flow field at the lower levels is smaller than 2% of the amplitude of the tangential wind analyzed by ECMWF due to the shallow penetration depth associated with the fine scale of the upper PV belt. Therefore, it is suggested that the added perturbation kinetic energy, as described by the principle of PV superposition (K. A. Emanuel 1988, personal communication), associated with the upper PV anomaly is not very significant in the intensification of Flo. This point will be elaborated further in section 5b.

On the other hand, according to the balanced vortex equations, the positive EFC produces a cyclonic vorticity tendency, and the vertical derivative of EFC can enhance the radial-vertical circulation inside the storm. We think that the strengthening of the radial-vertical circulation is more efficient than the spinup of the upper-tropospheric tangential wind in the process of storm intensification. The stronger outflow can take the high potential temperature air away from the core region, avoiding subsidence near the storm core, thus invigorating eyewall convection, and strengthening radial-vertical circulation. The increase in the low-level inflow can induce more moisture convergence, as well as additional energy from the ocean surface, which is favorable for storm intensification (Ooyama 1982). Additionally, the outflow also induced a compensated inflow near 400 hPa, which could help to maintain the vertical shear needed for development of the warm core.

One important factor that affects tropical cyclone intensity is the underlying sea surface temperature. Hence, we also look at the NCEP SST analyses (Fig. 2) and find that the SST is warm during the period of this case study. Moreover, the vertical wind shear is weak during this period. The warm underlying surface, the enhanced in-up-out circulation, and the weak vertical wind shear provide a suitable condition for the development of Flo, and thus Flo intensified rapidly before it became a Supertyphoon.

b. The intensification of Typhoon Gene

The intensification of Gene was identified to be associated with the approach of an upper-tropospheric trough. The evolution of PV in the outflow layer shows that the midlatitude trough, with a strip of high-PV air

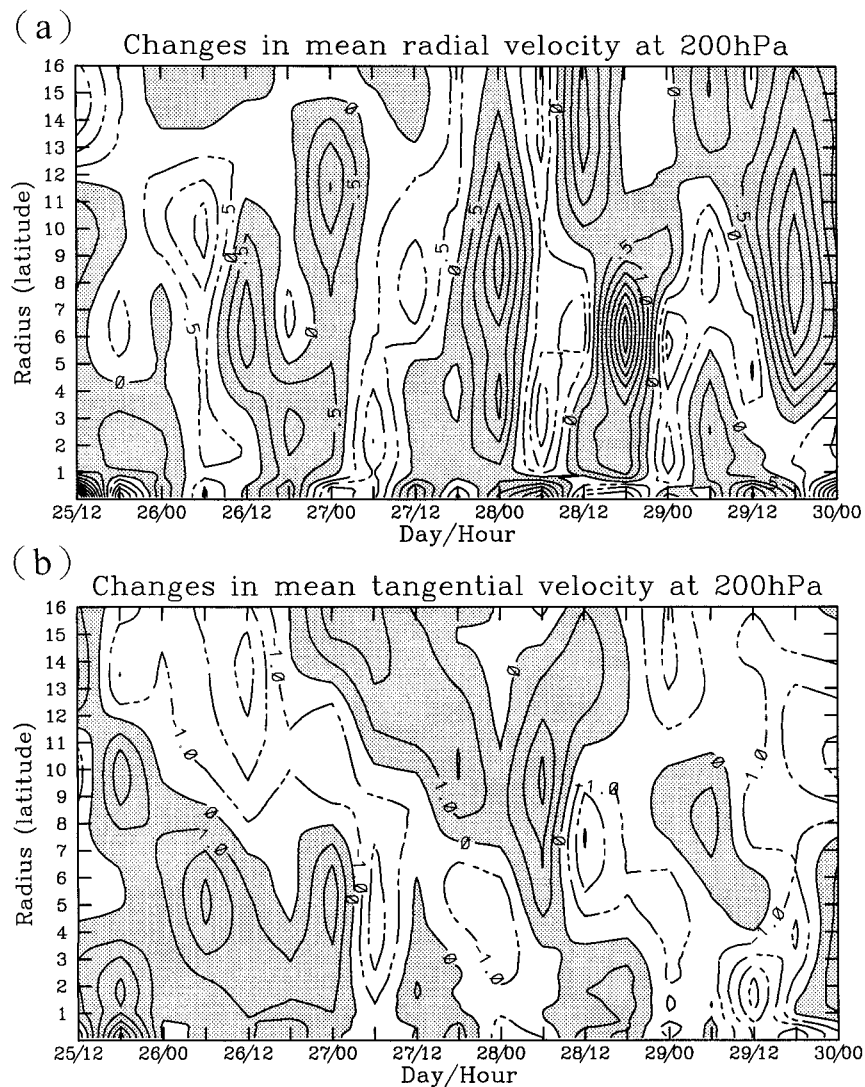


FIG. 19. As in Fig. 9 but for Typhoon Gene (1990).

extending to the northwest of the storm center, interacted with the outflow of Gene. The calculation of both the E-P flux and EFC shows that the interaction between the upper-tropospheric trough and Gene produced mean cyclonic angular momentum in the outflow layer. In addition, the outflow of Gene strengthened as the EFC appeared in the outflow layer. Gene began to intensify after a significant increase in the radial outflow at 200 hPa.

In theory, the interaction between the upper-tropospheric system and a tropical cyclone can produce EFC, which is favorable for the intensification of the tropical cyclone, but the approach of an upper-tropospheric trough also increases the vertical wind shear, which may be detrimental to its development. The result from the case study of Gene shows that the intensification was initiated before the trough moved to the north of the storm center. It is speculated that the interaction between

the outflow of Gene and the trough helped Gene to resist the negative effect associated with the large vertical wind shear.

One interesting question is: Is the intensification process of Gene similar to that of Hurricanes Elena (1985) and Danny (1985) as described in Molinari et al. (1995, 1998; cf. section 1c)? Namely, the interaction between the moving trough and the storm can be thought as the process of bringing two (upper- and lower-level) positive PV anomalies closer to each other. As indicated from the principle of PV superposition, the interaction between the upper- and lower-level positive PV anomalies can induce a transient growth of the total perturbation energy associated with the two systems. This process can initiate the WISHE instability (Emanuel 1991), thus leading to the storm intensification.

To quantify the above interaction process, piecewise PV inversion was also performed. It was found that,

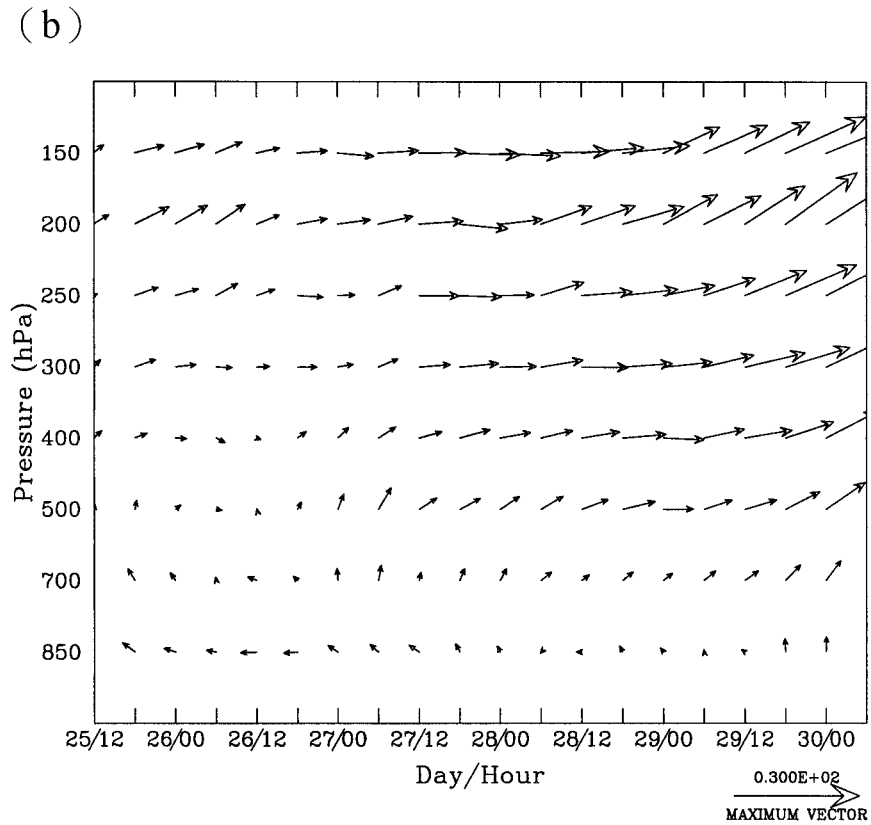
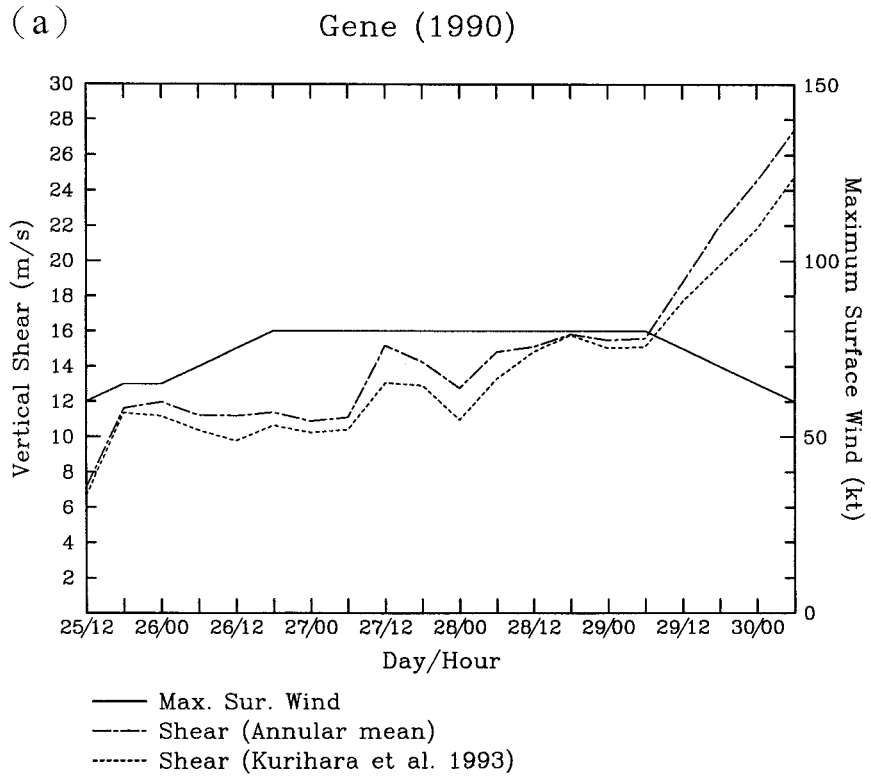


FIG. 20. As in Fig. 10 but for Typhoon Gene (1990).

because the upper PV anomaly (see Figs. 15b–d) either is not close enough to the storm center or has a too small horizontal scale, its associated balanced flow field (figures not shown) cannot penetrate downward to the lower storm center to result in a strong positive interference with the lower storm system. This result is not inconsistent with Molinari et al. (1995, 1998), which suggested that the thinning and scale reduction associated with the approaching upper-level positive PV anomaly was a key element in preventing the shear effect. However, our analysis further indicated that the ongoing interaction can be more complicated. Namely, the reduced-scale upper-level PV anomaly also becomes less effective in superposing its cyclonic circulation over the storm. Therefore, the typhoon–trough interaction, as interpreted from the concept of PV superposition, appears to be weak in our case studies.

6. Concluding remarks

In this paper, the ECMWF TOGA advanced analyses were used to study the environmental influences on the intensity of Typhoons Flo (1990) and Gene (1990). The axisymmetric structure and the evolution of PV and wind fields in the outflow layer are analyzed. The E–P flux, the eddy momentum flux convergence, and the mean vertical wind shear are computed in order to study the effects of the upper-level environmental forcings.

It is found that the axisymmetric PV in the outflow layer decreased with time as each typhoon intensified. The evolution of PV in the outflow layer also shows a low PV area over each typhoon, and these low PV areas expanded as the typhoons intensified. The PV structures of the two cases are consistent with the study by Wu and Emanuel (1994), where the PV sink in the outflow layer is represented as the expansion of the area of the negative upper-level PV anomaly.

The intensification of both Flo and Gene was associated with the influences of upper-level environmental features. The TUTT cell to the east of Flo provided an effective outflow channel and contributed to the upper-level EFC of angular momentum. The enhanced outflow, the upper-level EFC, the weak vertical wind shear, and the warm SST all provided favorable conditions for the development of Flo. As a result, Flo deepened rapidly and eventually became a supertyphoon, reaching a peak intensity of 75 m s^{-1} , which is about the empirical intensity upper bound associated with a SST of 28.2°C . On the other hand, the intensification of Gene was associated with its interaction with a midlatitude trough. The interaction between the trough and Gene produced upper-level EFC and induced the strengthening of the outflow.

Obviously, the difference in the intensity evolution between Flo and Gene not only arises from their different background SST distributions, but also from the different effects of the upper-level environmental forcings. Although the interaction between upper-tropo-

spheric systems and a tropical cyclone may add some cyclonic angular momentum into the cyclone vortex, such interactions do not ensure the intensification of tropical cyclones. In our case studies, the TUTT cell enhanced the outflow jet of Typhoon Flo, which encouraged the in–up–out circulation inside the storm, and then increased Flo’s deepening rate. However, the interaction between the midlatitude trough and the tropical cyclone not only provided the cyclonic angular momentum that may have led to Gene’s intensification, but also brought large vertical wind shear over Gene. The key factor that determines the result of the interaction appears to be the distance between the upper-level trough and the lower-level storm. We speculate that if the trough moves directly over the center of the storm, the strong vertical wind shear may tear the storm apart. While if the trough moves to the north of the storm at a distance, the preexisting outflow of the storm can interact with the trough and resist the effect of the vertical wind shear. Both the strengths and scales of the upper-level PV anomalies determine the vertical penetration depth of their associated circulations, and can result in different kinds of interaction.

The above results also show that as the tropical cyclone intensifies, the upper-level eddy momentum forcing is more important than the upper-level eddy heat forcing [this finding is consistent with Molinari et al. (1995)]. In other words, the EFC can be regarded as a good indication of the effect of the upper-level environmental forcing. It is found in this work that enhanced outflow favors the intensification of tropical cyclones, and constricted outflow inhibits the development of tropical cyclones. However, the existence of upper-level EFC does not ensure the strengthening of the outflow and the intensification of the tropical cyclone. The vertical wind shear also plays a subtle role, while the SST determines the thermodynamic potential of the storm intensity.

The above conclusion is deduced from the observational analyses of PV, EFC, vertical wind shear, and SST. Further investigation into the physical mechanisms of their mutual interaction can also be made through numerical simulations. However, the interaction between the environment and a typhoon involves complicated physical processes with multiple scale interactions, and these are difficult to characterize separately. For example, the study in this paper does not show whether Gene would intensify without the aforementioned trough interaction. Further fundamental advances in understanding the basic physics of typhoon intensity change are still needed. With the rapid improvement in computer capability, it is becoming possible for a numerical model to be able to fully simulate the full arrays of scales and physics that characterize tropical cyclones—that is, to simulate the individual cumulonimbus clouds that are the real agents of vertical transport in tropical cyclones (K. A. Emanuel 1998, personal communication), and to examine the atmosphere–ocean

interaction in a coupled typhoon model (I. Ginis 1998, personal communication). Progress in these directions should play important roles in improving intensity forecasts in the future.

This paper shows that the ECMWF operational analyses are useful for the study of the interaction between the synoptic features and the tropical cyclone. The importance of outflow dynamics has also been addressed in the case studies of Typhoons Flo and Gene. We think it is necessary to understand more about the outflow dynamics of tropical cyclones through better data sources. The use of operational analysis data, as well as retrieved winds along with temperature and moisture fields from satellites, can be very useful in providing better upper-tropospheric information. In the future, unmanned aircraft observations (Holland et al. 1992; Langford and Emanuel 1993) and GPS meteorological data (Rocken et al. 1995; Ware et al. 1996) may also provide more detailed wind, temperature, and moisture information both inside and around a tropical cyclone. It is hoped that a systematic combination of observational analyses and numerical model experiments can help improve our understanding of the interaction between a tropical cyclone and its environment, and aid in the prediction of tropical cyclone intensity.

Acknowledgments. The authors would like to thank three anonymous reviewers for their valuable suggestions. Helpful discussions with Drs. Cheng-Sheng Lee, Hung-Chi Kuo, and Ching-Yung Huang are appreciated. This work is supported the National Science Council of Taiwan by Grants NSC86-2111-M-002-009-API, NSC87-2111-M-002-004-API, and NSC88-2111-M-002-004-API.

REFERENCES

- Avila, L. A., 1998: Forecasting tropical cyclone intensity changes: An operational challenge. Preprints, *Symp. on Tropical Cyclone Intensity Change*, Phoenix, AZ, Amer. Meteor. Soc., 1–10.
- Bender, M. A., I. Ginis, and Y. Kurihara, 1993: Numerical simulations of tropical cyclone–ocean interaction with a high resolution coupled model. *J. Geophys. Res.*, **98**, 23 245–23 263.
- Black, P. G., and L. K. Shay, 1998: Observations of tropical cyclone intensity change due to air–sea interaction processes. Preprints, *Symp. on Tropical Cyclone Intensity Change*, Phoenix, AZ, Amer. Meteor. Soc., 161–168.
- Bosart, L. F., W. E. Bracken, J. Molinari, C. S. Velden, and P. Black, 1998: Environmental influence on the rapid intensification stage of Hurricane Opal (1995) over the Gulf of Mexico. Preprints, *Symp. on Tropical Cyclone Intensity Change*, Phoenix, AZ, Amer. Meteor. Soc., 105–112.
- Challa, M., and R. L. Pfeffer, 1980: Effects of eddy fluxes of angular momentum on model hurricane development. *J. Atmos. Sci.*, **37**, 1603–1618.
- De Maria, M., 1996: The effect of vertical shear on tropical cyclone intensity change. *J. Atmos. Sci.*, **53**, 2076–2087.
- , J.-J. Baik, and J. Kaplan, 1993: Upper-level eddy angular momentum fluxes and tropical cyclone intensity change. *J. Atmos. Sci.*, **50**, 1133–1147.
- Elsberry, R. L., 1990: International experiments to study tropical cyclones in the western North Pacific. *Bull. Amer. Meteor. Soc.*, **71**, 1305–1316.
- , B. C. Diehl, J. C.-L. Chan, P. A. Harr, G. J. Holland, M. Lander, T. Neta, and D. Thom, 1990: ONR Tropical Cyclone Motion Research Initiative: Field experiment summary. Naval Postgraduate School Report NPS-MR-91-001, Naval Postgraduate School, Monterey, CA, 107 pp.
- Emanuel, K. A., 1986: An air–sea interaction for tropical cyclones. Part I: Steady-state maintenance. *J. Atmos. Sci.*, **43**, 585–604.
- , 1988: The maximum intensity of hurricanes. *J. Atmos. Sci.*, **45**, 1143–1155.
- , 1991: The theory of hurricanes. *Annu. Rev. Fluid. Mech.*, **23**, 179–196.
- , 1995: Sensitivity of tropical cyclones to surface exchange coefficients and a revised steady-state model incorporating eye dynamics. *J. Atmos. Sci.*, **52**, 3969–3976.
- Gray, M. W., 1968: Global view of the origin of tropical disturbances and storms. *Mon. Wea. Rev.*, **96**, 669–700.
- Holland, G. J., 1997: The maximum potential intensity of tropical cyclones. *J. Atmos. Sci.*, **54**, 2519–2541.
- , and R. T. Merrill, 1984: On the dynamics of tropical cyclone structure changes. *Quart. J. Roy. Meteor. Soc.*, **110**, 723–745.
- , T. McGeer, and H. Youngren, 1992: Autonomous aerosondes for economical atmospheric sounding anywhere on the globe. *Bull. Amer. Meteor. Soc.*, **73**, 1987–1998.
- Kurihara, Y., M. A. Bender, and R. J. Ross., 1993: An initialization scheme of hurricane models by vortex specification. *Mon. Wea. Rev.*, **121**, 2030–2045.
- , R. E. Tuleya, and M. A. Bender, 1998: The GFDL hurricane prediction system and its performance in the 1995 hurricane seasons. *Mon. Wea. Rev.*, **126**, 1306–1322.
- Langford, J. S., and K. A. Emanuel, 1993: An unmanned aircraft for dropwindsonde development and hurricane reconnaissance. *Bull. Amer. Meteor. Soc.*, **74**, 367–375.
- McBride, J. L., 1981a: Observational analysis of tropical cyclone formation. Part I: Basic description of data sets. *J. Atmos. Sci.*, **38**, 1117–1131.
- , 1981b: Observational analysis of tropical cyclone formation. Part III: Budget analysis. *J. Atmos. Sci.*, **38**, 1152–1166.
- , and R. Zehr, 1981: Observational analysis of tropical cyclone formation. Part II: Comparison of non-developing versus developing systems. *J. Atmos. Sci.*, **38**, 1132–1151.
- Merrill, R. T., 1988: Environmental influences on hurricane intensification. *J. Atmos. Sci.*, **45**, 1678–1687.
- , and C. S. Velden, 1996: A three-dimensional analysis of outflow layer of Supertyphoon Flo (1990). *Mon. Wea. Rev.*, **124**, 47–63.
- Molinari, J., and D. Vollaro, 1989: External influences on hurricane intensity. Part I: Outflow layer eddy angular momentum fluxes. *J. Atmos. Sci.*, **46**, 1093–1105.
- , and —, 1990: External influences on hurricane intensity. Part II: Vertical structure and response of hurricane vortex. *J. Atmos. Sci.*, **47**, 1902–1918.
- , —, and F. Robasky, 1992: Use of ECMWF operational analyses for studies of the tropical cyclone environment. *Meteor. Atmos. Phys.*, **47**, 127–144.
- , S. Skubis, and D. Vollaro, 1995: External influences on hurricane intensity. Part III: Potential vorticity structure. *J. Atmos. Sci.*, **52**, 3593–3606.
- , —, —, F. Alsheimer, and H. E. Willoughby, 1998: Potential vorticity analysis of tropical cyclone intensification. *J. Atmos. Sci.*, **55**, 2632–2644.
- Montgomery, M. T., 1998: Vortex intensification by convectively forced Rossby waves. Preprints, *Symp. on Tropical Cyclone Intensity Change*, Phoenix, AZ, Amer. Meteor. Soc., 21.
- , and R. J. Kallenbach, 1997: A theory for the vortex Rossby waves and its application to spiral bands and intensity changes in hurricanes. *Quart. J. Roy. Meteor. Soc.*, **123**, 435–465.
- Ooyama, K. V., 1982: Conceptual evolution of the theory and modeling of the tropical cyclone. *J. Meteor. Soc. Japan*, **60**, 369–379.

- Pfeffer, R. L., and M. Challa, 1981: A numerical study of the role of eddy fluxes of momentum in the development of Atlantic hurricanes. *J. Atmos. Sci.*, **38**, 2392–2398.
- Rocken, C., T. VanHove, J. Johnson, F. Solheim, R. H. Ware, M. Bevis, S. Businger, and S. R. Chiswell, 1995: GPS/STORM-GPS sensing of atmospheric water vapor for meteorology. *J. Atmos. Oceanic Technol.*, **12**, 468–478.
- Rudolph, D. K., and C. P. Guard, 1990: Annual tropical cyclone report. Joint Typhoon Warning Center, Guam, Mariana Islands 280 pp.
- Shapiro, L. J., and H. E. Willoughby, 1982: The response of balanced hurricanes to local sources of heat and momentum. *J. Atmos. Sci.*, **39**, 378–394.
- Shay, L. K., G. Goni, F. Marks, J. Cione, and P. Black, 1998: Role of warm ocean features on intensity change. Preprints, *Symp. on Tropical Cyclone Intensity Change*, Phoenix, AZ, Amer. Meteor. Soc., 131–138.
- Sundqvist, H., 1970: Numerical simulation of the development of tropical cyclones with a ten-level model. Part I. *Tellus*, **22**, 369–390.
- Ware, R., and Coauthors, 1996: GPS sounding of the atmosphere from low Earth orbit: Preliminary results. *Bull. Amer. Meteor. Soc.*, **77**, 19–40.
- Willoughby, H. E., and P. G. Black, 1996: Hurricane Andrew in Florida: Dynamics of a disaster. *Bull. Amer. Meteor. Soc.*, **77**, 543–549.
- , J. A. Clos, M. G. Shoreibah, 1982: Concentric eyewalls, secondary wind maxima, and the evolution of the hurricane vortex. *J. Atmos. Sci.*, **39**, 395–411.
- Wu, C.-C., and K. A. Emanuel, 1993: Interaction of a baroclinic vortex with background shear: Application to hurricane movement. *J. Atmos. Sci.*, **50**, 62–76.
- , and —, 1994: On hurricane outflow structure. *J. Atmos. Sci.*, **51**, 1995–2003.
- , and —, 1995: Potential vorticity diagnostics of hurricane movement. Part I: A case study of Hurricane Bob (1991). *Mon. Wea. Rev.*, **123**, 69–92.
- , and Y. Kurihara, 1996: A numerical study of the feedback mechanism of hurricane–environment interaction on hurricane movement from the potential vorticity perspective. *J. Atmos. Sci.*, **53**, 2264–2282.